Electronic Supplementary Material (ESI) for ChemComm.
This journal is © The Royal Society of Chemistry 2018

Supporting Information for

Anion–π Interactions of Highly π-Acidic Dipyridinium-Naphthalene Diimide Salts

Teck Lip Dexter Tam,[*#a] Chee Koon Ng,[#a] Xuefeng Lu,[b] Zheng Long Lim,[b] Jishan Wu[*a,b]

[a] *Institute of Materials Research and Engineering (IMRE), Agency of Science, Technology and Research (A*STAR), 2 Fusionopolis Way, Innovis, #08-03, Singapore 138634, Singapore*

[b] *Department of Chemistry, National University of Singapore, 3 Science Drive 3, 117543, Singapore*

Table of Contents

1. Experimental section ····· S2
   1.1 General ····· S2
   1.2 Synthetic procedures and characterization data ····· S3
2. Proposed decomposition pathway of Py_2-NDI•2F ····· S7
3. X-ray crystallographic structures, selected crystal data, data collection, and refinement parameters ····· S10
4. Characterization data of Py_2-NDI•2X salts ····· S13
5. ^{1}H, ^{13}C{^{1}H} NMR, MALDI-TOF and ESI mass spectra of synthesized compounds ····· S19
6. References ····· S47

1. Experimental Section

1.1. General

All reagents were purchased from Sigma Aldrich other than 2,6-dibromo-*N*,*N*'-bis(2-ethylhexyl)-1,8:4,5-naphthalene tetracarboxdiimide (TCI). ^{1}H and ^{13}C{^{1}H} NMR were performed on JEOL 500MHz NMR system with chemical shifts referenced to the deuterated solvent. The ^{19}F, ^{35}Cl, ^{81}Br and ^{127}I NMR spectra were recorded on a JEOL 500MHz NMR operating at 470.39, 49.94, 134.89 and 99.94 MHz for ^{19}F, ^{35}Cl, ^{81}Br and ^{127}I respectively. The ^{19}F, ^{35}Cl, ^{81}Br and ^{127}I NMR spectra were externally referenced to 1.0 M aqueous (D_2O) solutions of KF, NaCl, NaBr and NaI respectively, at 0 ppm. Variable-temperature ^{1}H NMR was performed on Bruker DPX 400 MHz spectrometer. Matrix assisted laser desorption/ionization time-of-flight (MALDI-TOF) mass spectra were obtained on a Bruker Daltonics Autoflex II TOF/TOF system. Elemental analysis was carried out using CHNS FlashEA 1112 Elemental Analyzer from Thermo Fisher Scientific. UV-Vis-NIR absorption spectra were recorded on a Shimadzu UV-3101PC UV-VIS-NIR Spectrophotometer. Cyclic voltammetry (CV) experiments were performed using Autolab potentiostat (model PGSTAT30) by Echochimie. All CV measurements were recorded in dry acetonitrile with 0.1 M tetra-*n*-butylammonium hexafluorophosphate as supporting electrolyte (scan rate of 100 mV•s^{-1}), glassy carbon disk as working electrode, gold disk as counter electrode and Ag/AgCl as reference electrode. Ferrocene was used as external standard (HOMO = oxidation onset = –4.80 eV). LUMO values of the compounds were calculated using the formula: –4.80 – (reduction onset of compound). Continuous wave X-band ESR spectra were obtained with a JEOL (FA200) spectrometer at room temperature using dry dichloromethane as solvent and DPPH as standard. XPS spectra were measured on powder samples using VG Thermo Escalab 220i -XL X-ray photoelectron spectroscopy system. XPS data is analyzed using Thermo Avantage v4.12. Single crystals were submitted to X-ray Diffraction Laboratory in National University of Singapore for single crystal structure. ESI-MS measurements were performed on Shimadzu LCMS-IT-TOF, isotope distribution patterns were used as a composition proof in addition to m/z signal.

1.2. Synthetic procedures and characterization data

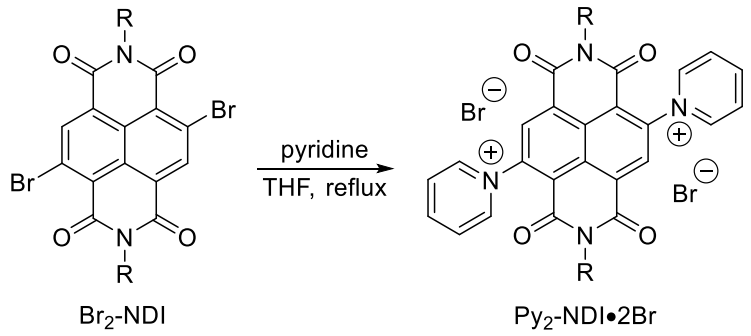

R = 2-ethylhexyl

Py_2-NDI•2Br. 500 mg of 2,6-dibromo-*N*,*N*'-bis(2-ethylhexyl)-1,8:4,5-naphthalene tetracarboxdiimide (Br_2-NDI, 0.77 mmol), 50 mL of THF and 1.24 mL of pyridine (15.33 mmol) was added into a two-necked round-bottom flask with a condenser attached. The reaction setup was purged with nitrogen and refluxed for 24 hours. At the end of the reaction, the reaction mixture was filtered and washed with THF. The solids were re-dissolved in methanol, filtered and the filtrate was concentrated. The concentrated methanol solution precipitated in toluene, filtered, washed with toluene and dried under vacuum. Yield: 466 mg (75%). Orange solids. Single crystals were obtained by layering diethyl ether on a concentrated solution of Py_2-NDI•2Br in ethanol. ^{1}H NMR (500 MHz, DMSO-d_6) δ 9.41 (dd, J = 6.5, 1.2 Hz, 4H), 9.22 (s, 2H), 8.98 (tt, J = 7.9, 1.3 Hz, 2H), 8.49 – 8.45 (m, 4H), 3.92 – 3.83 (m, 4H), 1.76 – 1.68 (m, 2H), 1.32 – 1.18 (m, 16H), 0.85 – 0.80 (m, 12H). ^{13}C{^{1}H} NMR (125 MHz, DMSO-d_6) δ 161.13, 160.59, 148.31, 145.85, 142.79, 131.55, 127.89, 127.42, 127.27, 121.47, 43.96, 37.02, 29.71, 27.70, 23.11, 22.42, 13.94, 10.23. Anal. Calcd for $C_{40}H_{46}Br_2N_4O_4$: C, 59.56; H, 5.75; Br, 19.81; N, 6.95; O, 7.93. Found: C, 59.68; H, 5.71; N, 6.88. MALDI-TOF-MS *m*/*z*: 646.38 (M^+-2Br); calcd. for $C_{40}H_{46}N_4O_4$ (M^+-2Br) = 646.35.

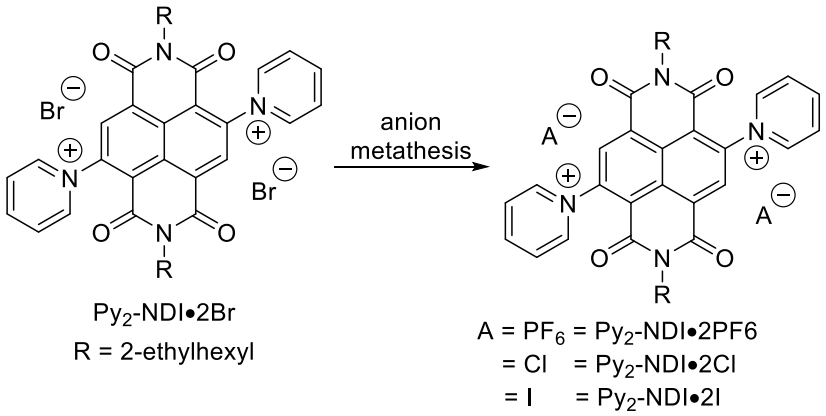

Py_2-NDI•2PF_6. 100 mg of Py_2-NDI•2Br were dissolved in 4 mL of saturated methanolic ammonium hexafluorophosphate solution. The solution was mixed well and precipitated in 100 mL of DI water. The precipitate was filtered, washed with DI water followed by minimum methanol and dried under vacuum. Yield: 82 mg (70%). White solids. Single crystals were obtained by layering diethyl ether on a concentrated solution of Py_2-NDI.2PF_6 in acetonitrile. ^{1}H NMR (500 MHz, DMSO-d_6) δ 9.38 (dd, J = 6.2, 1.0 Hz, 4H), 9.22 (s, 2H), 8.98 (tt, J = 8.0, 1.3 Hz, 2H), 8.48 – 8.45 (m, 4H), 3.93 – 3.84 (m, 4H), 1.74 – 1.69 (m, 2H), 1.32 – 1.15 (m, 16H), 0.85 – 0.80 (m, 12H). ^{13}C{^{1}H} NMR (125 MHz, DMSO-d_6) δ 161.10, 160.57, 148.36, 145.84, 142.92, 131.60, 127.91, 127.40, 127.22, 121.41, 43.93, 37.06, 29.70, 27.69, 23.09, 22.42, 13.93, 10.22. Anal. Calcd for $C_{40}H_{46}F_{12}N_4O_4P_2$: C, 51.29; H, 4.95; F, 24.34; N, 5.98; O, 6.83; P, 6.61. Found: C, 51.48; H, 5.11; N, 6.23. MALDI-TOF-MS m/z: 645.86 (M^+-2PF_6); calcd. for $C_{40}H_{46}N_4O_4$ (M^+-2PF_6) = 646.35.

Py_2-NDI•2Cl. 80.6 mg of Py_2-NDI•2Br (0.1 mmol) was dissolved in 2 mL of methanol. 40 mg of silver chloride (0.4 mmol) was added and the suspension was sonicated in the dark for 30 mins. The suspension was allowed to stir overnight under light illumination. The reaction was filtered through 0.45 μm PTFE filter and solvent was removed using rotary evaporation. The solids were washed with toluene and dried under vacuum. Single crystals were obtained by layering diethyl ether on a concentrated solution of Py_2-NDI•2Cl in ethanol. Yield: 59 mg (82%). Yellow solids. ^{1}H NMR (500 MHz, DMSO-d_6) δ 9.45 (dd, J = 6.6, 1.0 Hz, 4H), 9.22 (s, 2H), 8.98 (tt, J = 7.9, 1.3 Hz, 2H), 8.49 – 8.45 (m, 4H), 3.92 – 3.83 (m, 4H), 1.74 – 1.69 (m, 2H), 1.32 – 1.18 (m, 16H), 0.84 – 0.79 (m, 12H). ^{13}C{^{1}H}

NMR (125 MHz, DMSO-d_6) δ 161.13, 160.59, 148.31, 145.89, 142.84, 131.56, 127.90, 127.42, 127.26, 121.47, 43.95, 37.04, 29.72, 27.70, 23.11, 22.43, 13.95, 10.23. Anal. Calcd for $C_{40}H_{46}Cl_2N_4O_4$: C, 66.94; H, 6.46; Cl, 9.88; N, 7.81; O, 8.92. Found: C, 66.68; H, 6.19; N, 7.63. MALDI-TOF-MS *m*/*z*: 645.96 (M^+-2Cl); calcd. for $C_{40}H_{46}N_4O_4$ (M^+-2Cl) = 646.35.

Py_2-NDI•2I. 100 mg of Py_2-NDI•2Br were dissolved in 2 mL of saturated methanolic sodium iodide solution. The solution was stirred for 2 mins and precipitated in 100 mL of DI water. The precipitate was filtered, washed with DI water and dried under vacuum. Yield: 85 mg (76 %). Violet solids. Single crystals were obtained by layering diethyl ether on a concentrated solution of Py_2-NDI•2I in ethanol. ^{1}H NMR (500 MHz, DMSO-d_6) δ 9.40 (d, *J* = 5.8 Hz, 4H), 9.22 (s, 2H), 8.98 (t, *J* = 7.9 Hz, 2H), 8.49 – 8.45 (m, 4H), 3.92 – 3.83 (m, 4H), 1.74 – 1.69 (m, 2H), 1.34 – 1.16 (m, 16H), 0.84 – 0.79 (m, 12H). ^{13}C{^{1}H} NMR (125 MHz, DMSO-d_6) δ 148.34, 145.85, 127.94, 43.96, 37.02, 29.70, 27.68, 23.10, 22.42, 13.93, 10.22. Anal. Calcd for $C_{40}H_{46}I_2N_4O_4$: C, 53.34; H, 5.15; I, 28.18; N, 6.22; O, 7.11. Found: C, 53.58; H, 5.21; N, 6.33. MALDI-TOF-MS *m*/*z*: 646.16 (M^+-2I); calcd. for $C_{40}H_{46}N_4O_4$ (M^+-2I) = 646.35.

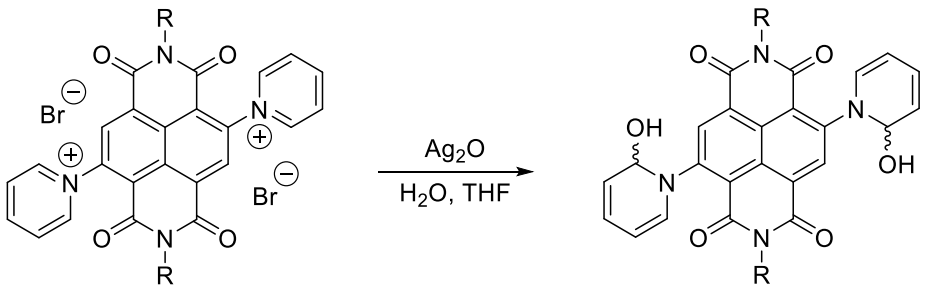

Py2-NDI·2Br
R = 2-ethylhexyl

Py2-NDI·2OH

Py_2.NDI•2OH. 115 mg of Py_2.NDI•2Br (0.14 mmol) and 66 mg of Ag_2O (0.28 mmol) were suspended in 50 mL of THF and 10 mL of DI water. The reaction was stirred for two hours and filtered through celite. Solvent was removed from the filtrate and the residue was washed with DI water. The compound was purified using column chromatography (100% dichloromethane → 98% dichloromethane + 2% methanol). Yield: 69 mg (71%). Dark blue solids. ^{1}H NMR (500 MHz, CD_2Cl_2) δ 11.98 (d, *J* = 12.2 Hz, 2H), 9.54 (d, *J* = 9.6 Hz, 2H),

8.56 (s, 2H), 7.69 (t, *J* = 12.6 Hz, 2H), 7.30 (t, *J* = 13.6 Hz, 2H), 6.34 (t, *J* = 12.7 Hz, 2H), 6.13 (dd, *J* = 15.4, 8.4 Hz, 2H), 4.20 – 4.06 (m, 4H), 1.97 – 1.86 (m, 2H), 1.47 – 1.23 (m, 16H), 0.94 (t, *J* = 6.0 Hz, 6H), 0.92 – 0.86 (m, 6H). $^{13}C\{^{1}H\}$ NMR (125 MHz, CD_2Cl_2) δ 193.20, 166.95, 162.89, 151.48, 143.59, 136.00, 128.66, 126.89, 123.43, 119.71, 112.00, 105.20, 44.95, 38.50, 31.28, 29.23, 24.60, 23.63, 14.43, 10.97. Anal. Calcd for $C_{40}H_{48}N_4O_6$: C, 70.56; H, 7.11; N, 8.23; O, 14.10. Found: C, 70.33; H, 7.00; N, 8.23. MALDI-TOF-MS *m*/*z*: 680.96 (M^+); calcd. for $C_{40}H_{48}N_4O_6$ = 680.36.

2. Proposed decomposition pathway of Py_2-NDI•2F

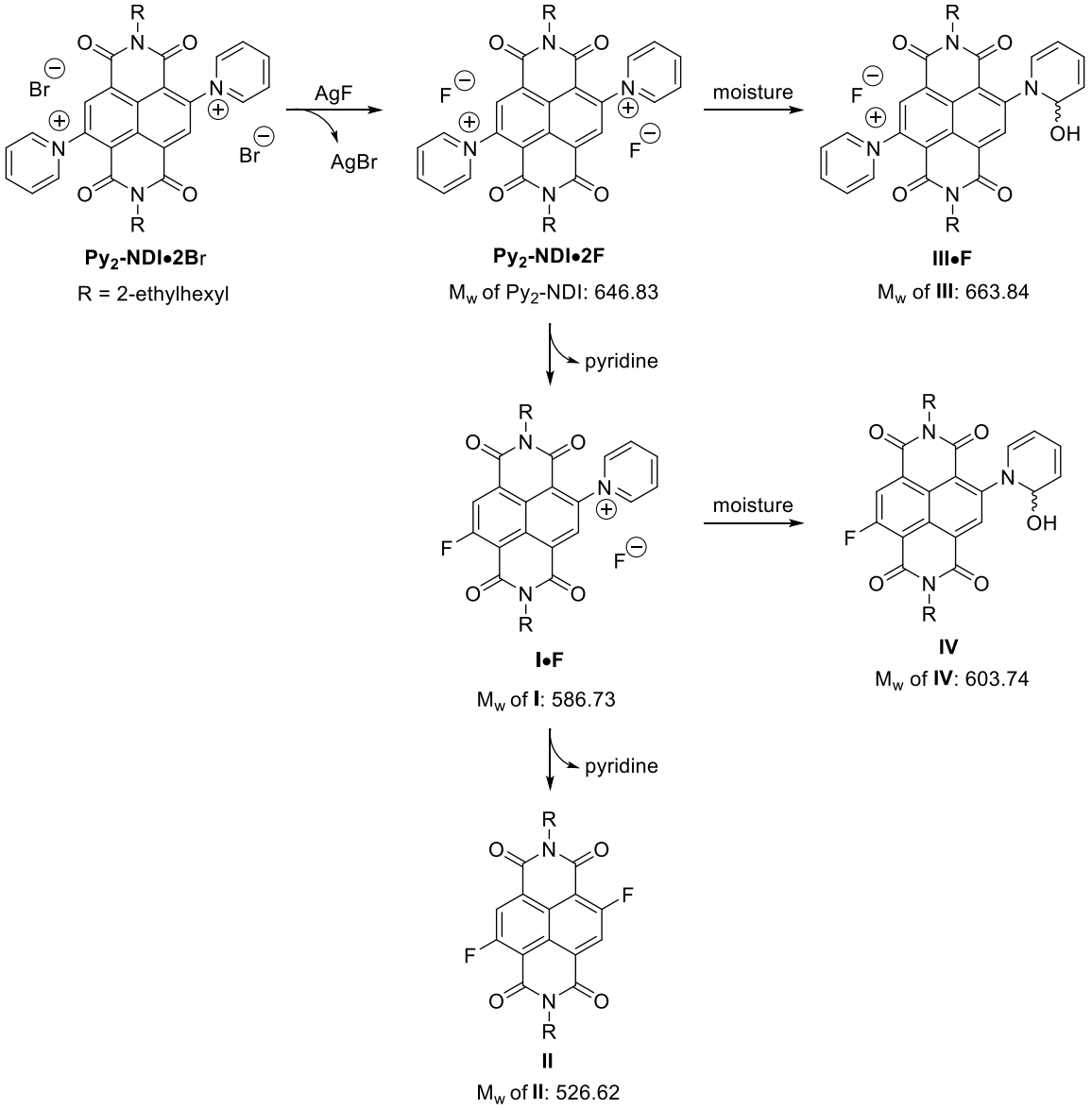

Figure S1. Proposed decomposition pathway of **Py_2-NDI•2F**. **Py_2-NDI•2F** decomposes via nucleophilic aromatic substitution to form **I.F** and **II**. However, in the presence of atmospheric moisture, **III.F** and **IV** are also formed.

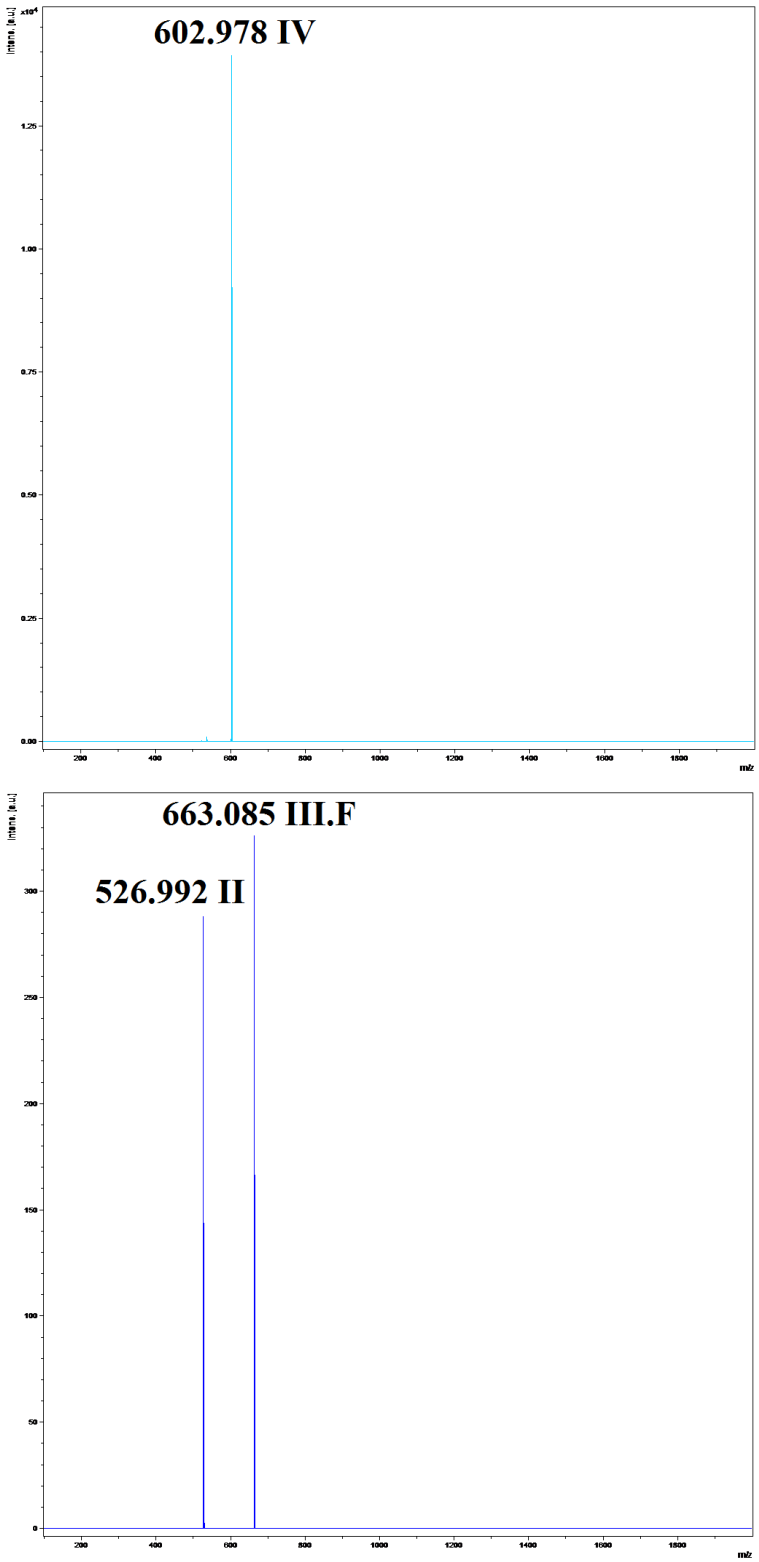

Figure S2. MALDI-TOF mass spectrum of crude reaction mixture as shown in **Figure S1**. Top: positive mode, bottom: negative mode.

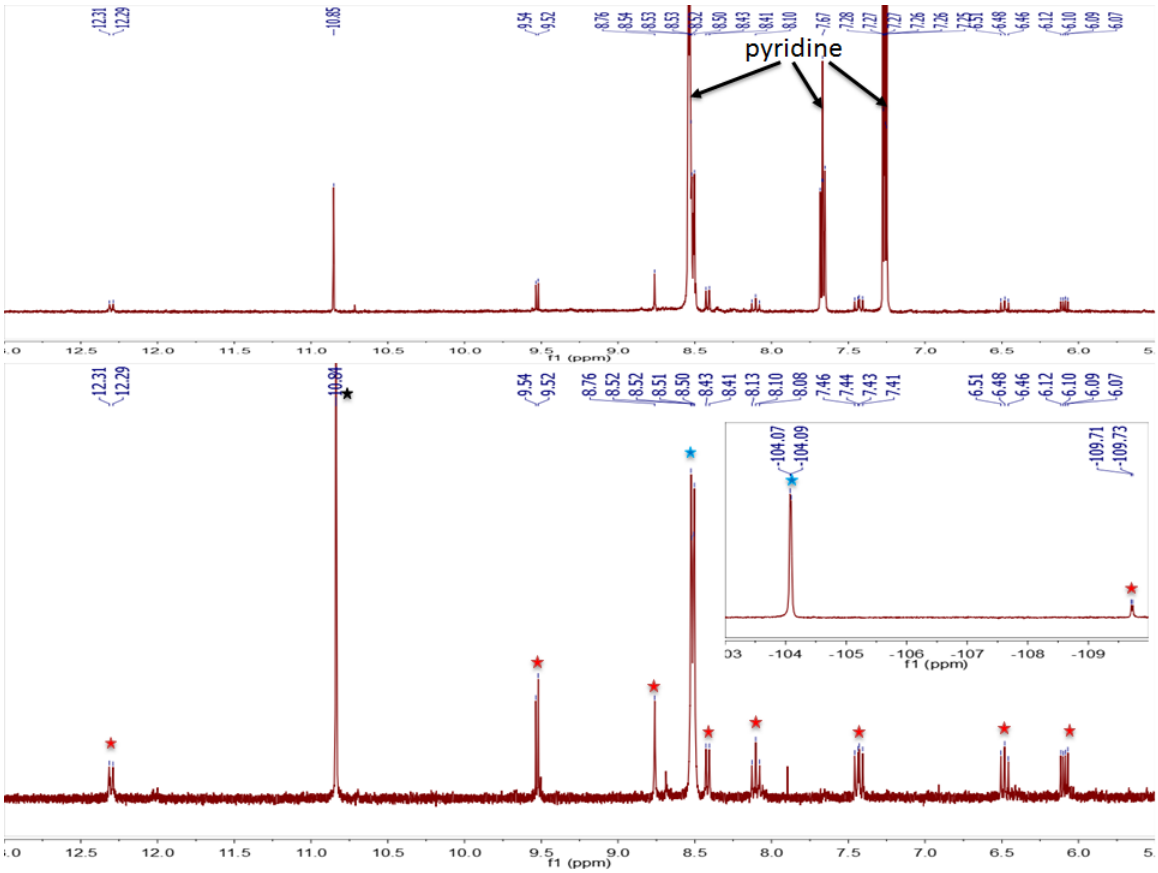

Figure S3. Top: ^{1}H NMR of crude reaction mixture as shown in **Figure S1**. Bottom: ^{1}H NMR of crude reaction mixture as shown in **Figure S1** after removal of pyridine. Inset: ^{19}F NMR of crude reaction mixture as shown in **Figure S1**. Red star: peaks corresponding to **IV**, blue star: peaks corresponding to **II**, black star: unknown impurity. **Py$_2$-NDI•2F**, **I•F** and **III•F** are NMR silent.

3. X-ray crystallographic structures, selected crystal data, data collection, and refinement parameters

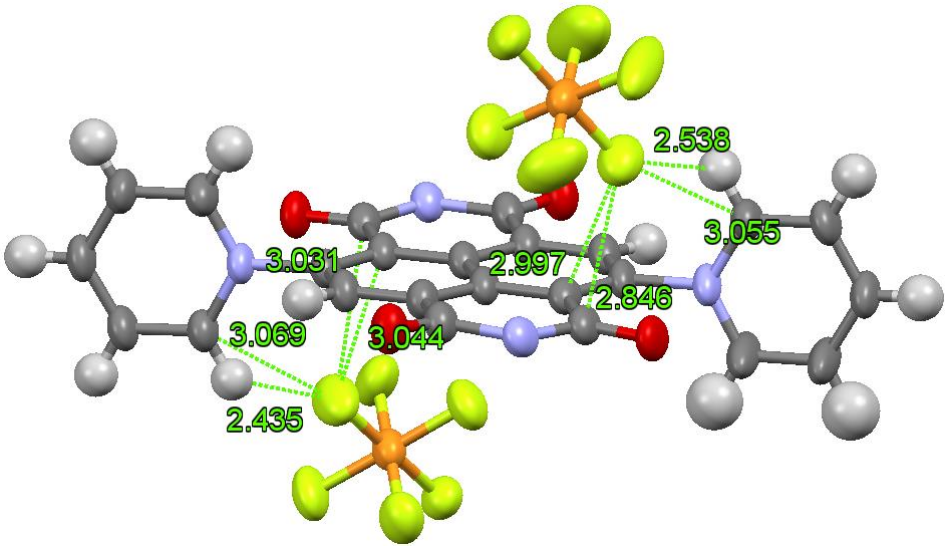

Figure S4. X-ray crystallographic structure of Py_2-NDI•$2PF_6$ showing PF_6^- above and below the NDI core. Alkyl groups are omitted for clarity. [C–H•••F] short contact distances: 2.435 and 2.538 Å, [C•••F] short contact distances: 3.069, 3.031, 3.044, 3.055, 2.997 and 2.846 Å.

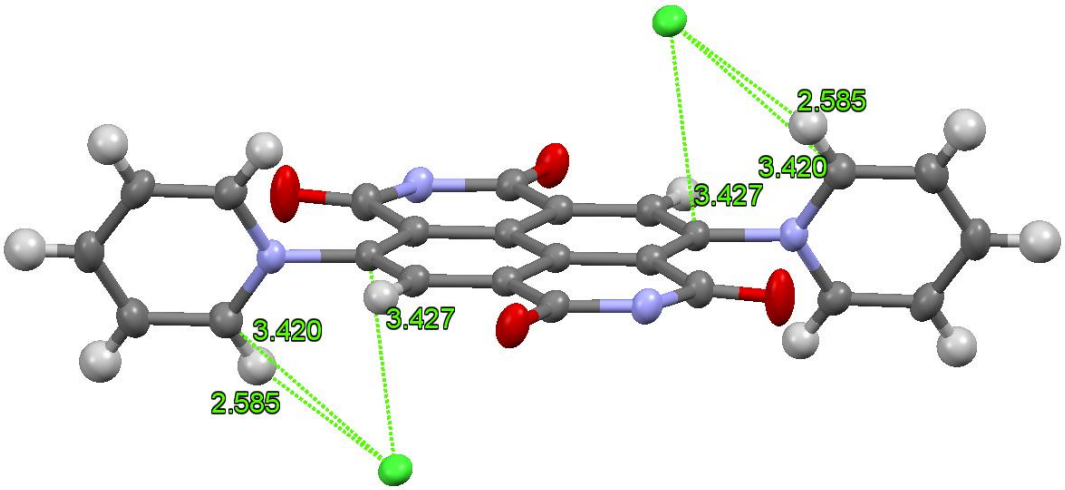

Figure S5. X-ray crystallographic structure of Py_2-NDI•2Cl showing Cl^- above and below the NDI core. Alkyl groups are omitted for clarity. [C–H•••Cl^-] short contact distances: 2.585 Å, [C•••Cl^-] short contact distances: 3.420 and 3.427 Å.

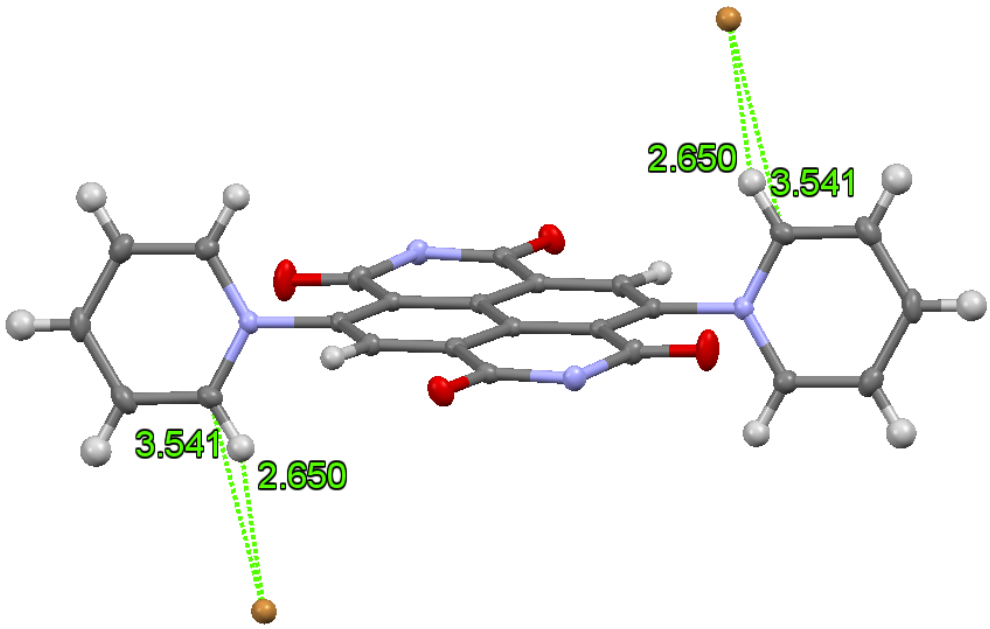

Figure S6. X-ray crystallographic structure of Py_2-NDI•2Br showing Br^- above and below the NDI core. Alkyl groups are omitted for clarity. [C–H•••Br^-] short contact distance: 2.650 Å, [C•••Br^-] short contact distance: 3.541 Å.

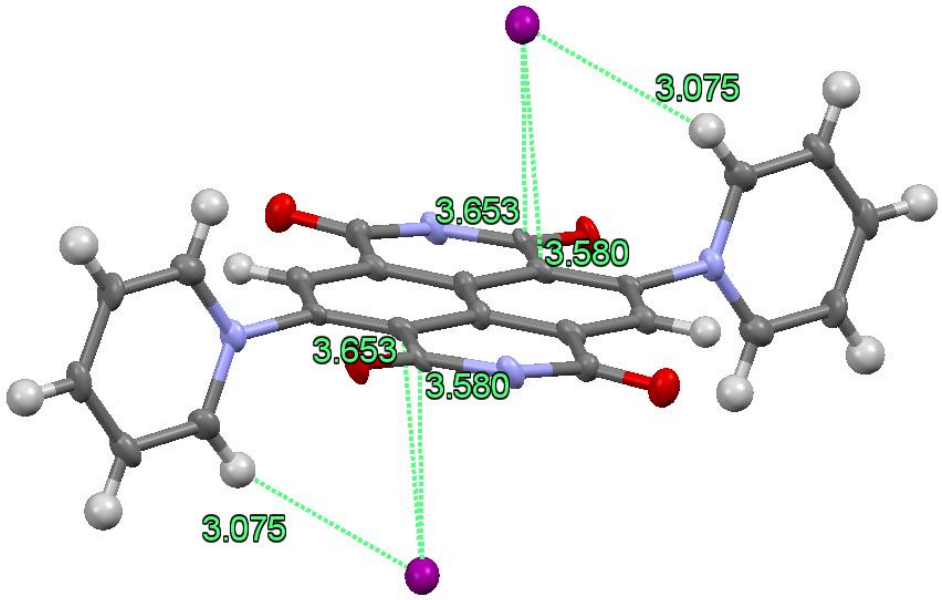

Figure S7. X-ray crystallographic structure of Py_2-NDI•2I showing I^- above and below the NDI core. Alkyl groups are omitted for clarity. [C–H•••I^-] short contact distance: 3.075 Å, [C•••I^-] short contact distances: 3.580 and 3.653 Å.

	Py_2-NDI•2Cl	**Py_2-NDI•2Br**	**Py_2-NDI•2I**	**Py_2-NDI•2PF_6**
Empirical formula	$C_{44}H_{58}Cl_2N_4O_6$	$C_{44}H_{58}Br_2N_4O_6$	$C_{44}H_{58}I_2N_4O_6$	$C_{46}H_{52}F_{12}N_7O_4P_2$
Formula weight	809.84	898.76	992.74	1059.91
Temperature of data collection	100(2) K	100(2) K	100(2) K	100(2) K
Wavelength	1.54178 Å	0.71073 Å	1.54178 Å	1.54178 Å
Crystal size	0.286 x 0.175 x 0.072 mm^3	0.60 x 0.46 x 0.12 mm^3	0.070 x 0.092 x 0.118 mm^3	0.318 x 0.211 x 0.060 mm^3
Crystal system	Triclinic	Monoclinic	Triclinic	Monoclinic
Space group	P-1	$P2_1/c$	P -1	$P2_1/c$
Unit cell dimensions	a = 7.9255(5) Å α = 96.993(2)° b = 9.2590(6) Å β = 98.728(2)° c = 15.1784(9) Å γ = 98.758(2)°	a = 8.3030(10) Å α = 90° b = 28.106(4) Å β = 104.697(2)° c = 9.5912(12) Å γ = 90°	a = 9.0399(6) Å α = 84.915(4)° b = 10.7529(7) Å β = 70.321(4)° c = 12.1907(8) Å γ = 80.746(4)°	a = 12.6980(5) Å α = 90° b = 17.0155(8) Å β = 96.201(2)° c = 23.0412(10) Å γ = 90°
Volume	1076.06(12) $Å^3$	2165.0(5) $Å^3$	1100.51(13) $Å^3$	4949.2(4) $Å^3$
Z	1	2	2	4
Density (calculated)	1.250 g/cm^3	1.379 g/cm^3	1.498 g/cm^3	1.418 g/cm^3
F(000)	432	936	504	2188
Theta range for data collection	4.887 to 70.365°	1.449 to 27.497°	3.85 to 65.47°	3.501 to 66.573°
Reflections collected	14083	35480	8928	39546
Independent reflections	4071 [R(int) = 0.0389]	4982 [R(int) = 0.0473]	3571 [R(int) = 0.0476]	8710 [R(int) = 0.0554]
Goodness-of-fit on F^2	1.093	1.047	1.082	1.022
Final R indices [I>2sigma(I)]	R1 = 0.0630, wR2 = 0.1710	R1 = 0.0317, wR2 = 0.0776	R1 = 0.0496, wR2 = 0.1050	R1 = 0.0901, wR2 = 0.2703
R indices (all data)	R1 = 0.0645, wR2 = 0.1726	R1 = 0.0358, wR2 = 0.0795	R1 = 0.0652, wR2 = 0.1139	R1 = 0.1010, wR2 = 0.2855
Largest diff. peak and hole	1.360 and -0.858 e.$Å^{-3}$	0.563 and -0.320 e.$Å^{-3}$	1.114 and -1.173 e$Å^{-3}$	1.220 and -0.768 e.$Å^{-3}$

Table S1. Selected crystal data, data collection, and refinement parameters for **Py_2-NDI•2Cl**, **Py_2-NDI•2Br**, **Py_2-NDI•2I** and **Py_2-NDI•2PF_6**.

4. Characterization data of Py_2-NDI•2X salts

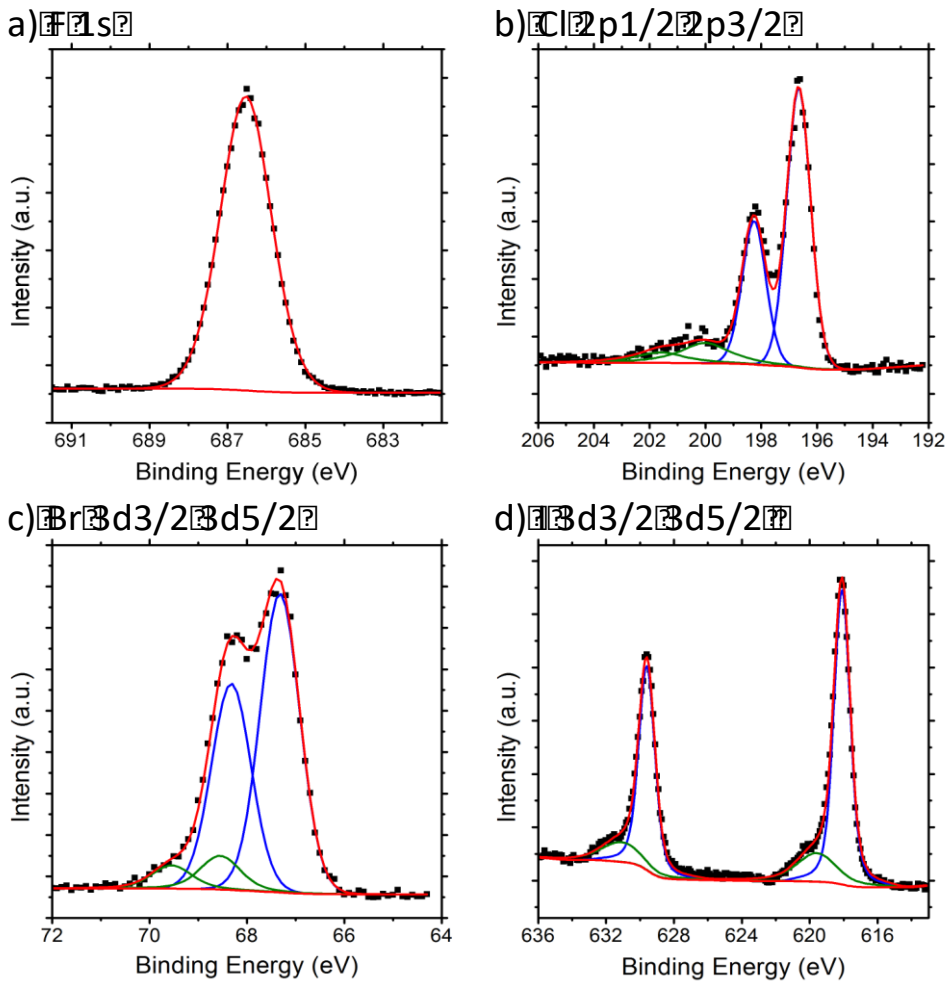

Figure S8. XPS of a) Py_2-NDI•PF_6, b) Py_2-NDI•2Cl, c) Py_2-NDI•Br and d) Py_2-NDI•2I.

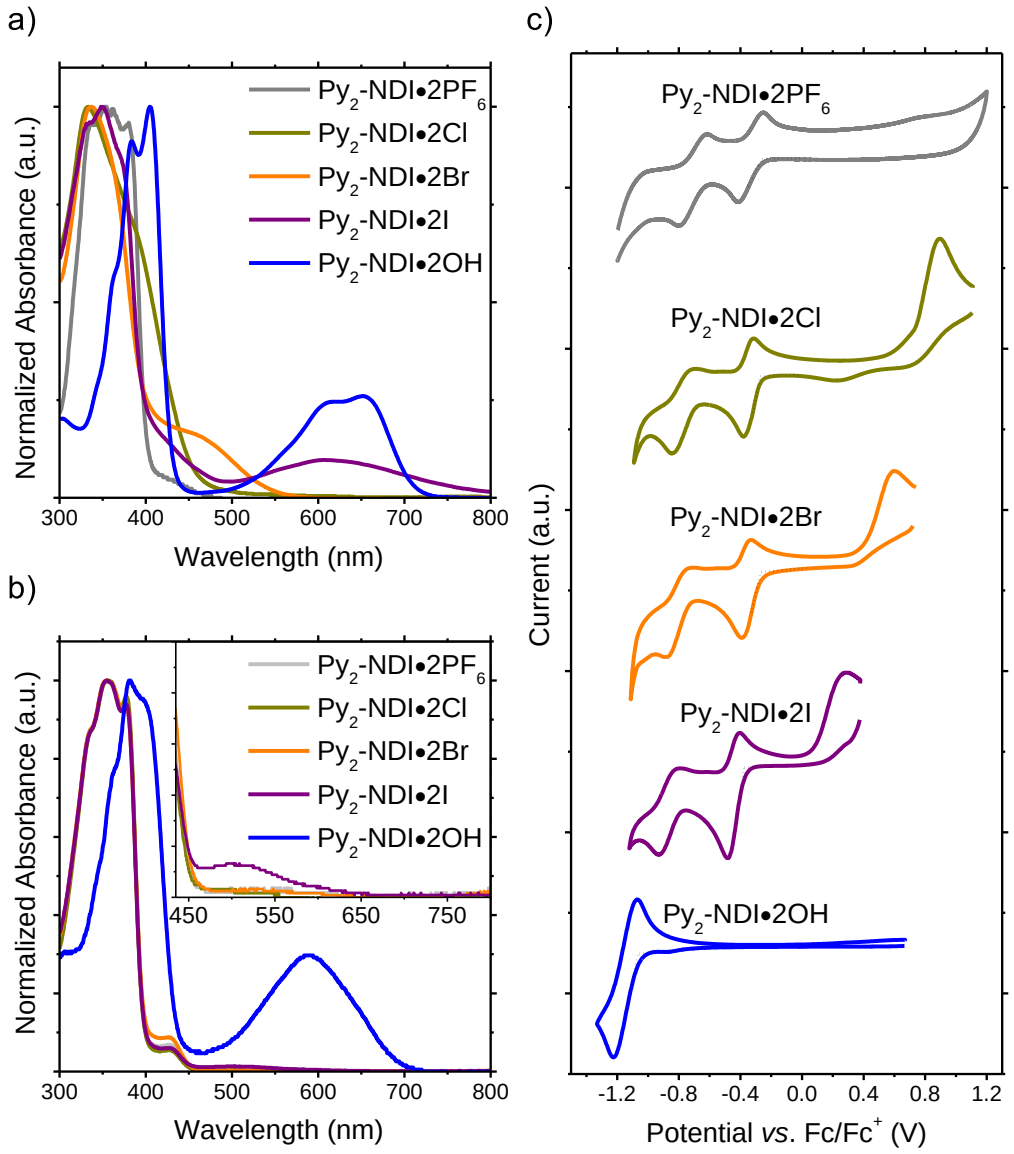

Figure S9. Solution UV-Vis absorption spectra in a) $CHCl_3$ and b) CH_3OH. c) Solution cyclic voltammograms in CH_3CN.

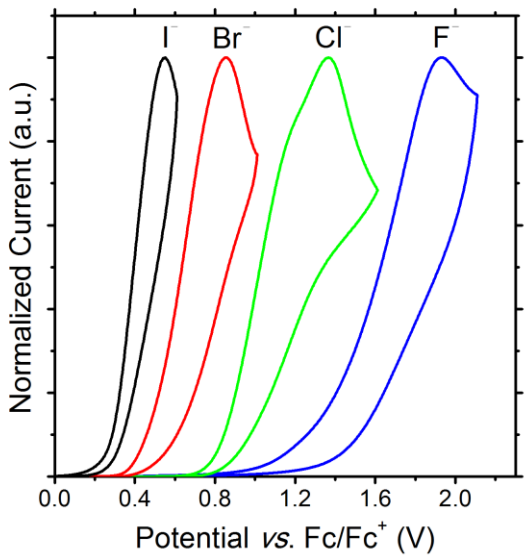

Figure S10. Solution cyclic voltammograms of tetra-*n*-butylammonium halides in acetonitrile.

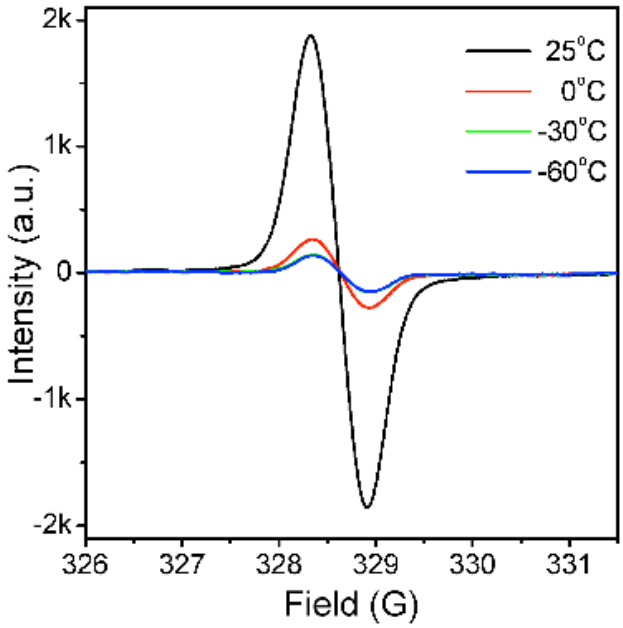

Figure S11. Variable temperature electron paramagnetic resonance spectra of Py_2-NDI•2I in CH_2Cl_2.

DFT calculation was carried out using the Gaussian 09 program suite.[1] Geometry optimization in the gas phase was performed to obtain the monoradical monocation. Subsequent single-point energy calculation was carried out on the gas phase optimized structure using solvation model. Level of theory: DFT UB3LYP 6-31G (d,p). Solvation model: IEF-PCM (acetonitrile).

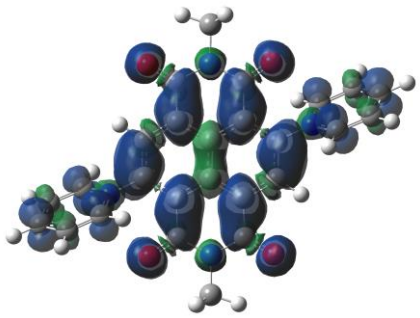

Figure S12. Electron transfer from iodide to Py_2-NDI^{2+} will generate Py_2-$NDI^{+\bullet}$ with spin density mainly located on the NDI core. Low spin density was found on the pyridinium carbons, especially C3.

	Temp (°C)	Chemical Shift of Py_2-NDI•2X (ppm)	$LW_{1/2}$ (Hz)	Chemical Shift of TBA•X (ppm)	$LW_{1/2}$ (Hz)
PF_6^- (^{19}F)	25	–72.29, –73.80	2	–72.29, –73.80	2
	70	–70.87, –72.38	2	–70.88, –72.39	2
Cl^- (^{35}Cl)	25	72.79	90	70.66	35
	70	72.45	49	69.42	8
Br^- (^{81}Br)	25	165.93	1405	160.78	375
	70	162.85	992	156.51	216
I^- (^{127}I)	25	- [a]	- [a]	186.91	1488
	70	- [a]	- [a]	195.39	700

Table S2. ^{19}F, ^{35}Cl, ^{81}Br, and ^{127}I NMR chemical shifts and $LW_{1/2}$ of TBA•X and Py_2-NDI•2X where X = PF_6, Cl, Br and I at 25 °C and 70 °C. All halogen NMR were performed in DMSO-d_6. $LW_{1/2}$: line width at half height. [a] ^{127}I NMR signal not observed, likely due to the I^- being bounded to the Py_2-NDI^{2+}, resulting severe peak broadening, or partial electron being transferred from I^- to Py_2-NDI^{2+}, resulting in a radical $I^\bullet$ species invisible to NMR.

5. ^{1}H, ^{13}C{^{1}H} NMR, MALDI-TOF and ESI mass spectra of synthesized compounds

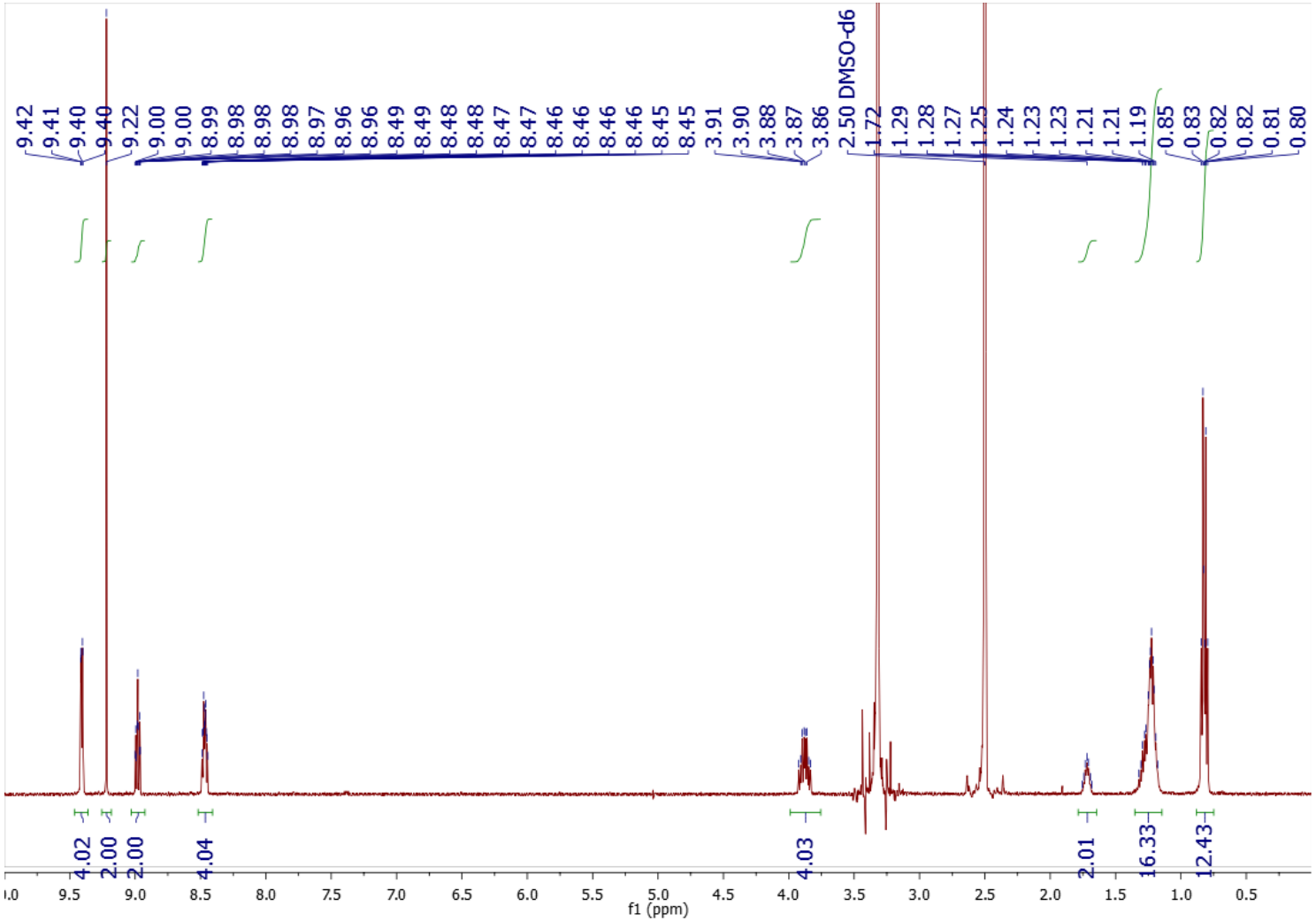

Figure S13. ^{1}H NMR spectrum (500 MHz) of **Py$_2$-NDI•2Br** in DMSO-*d*$_6$.

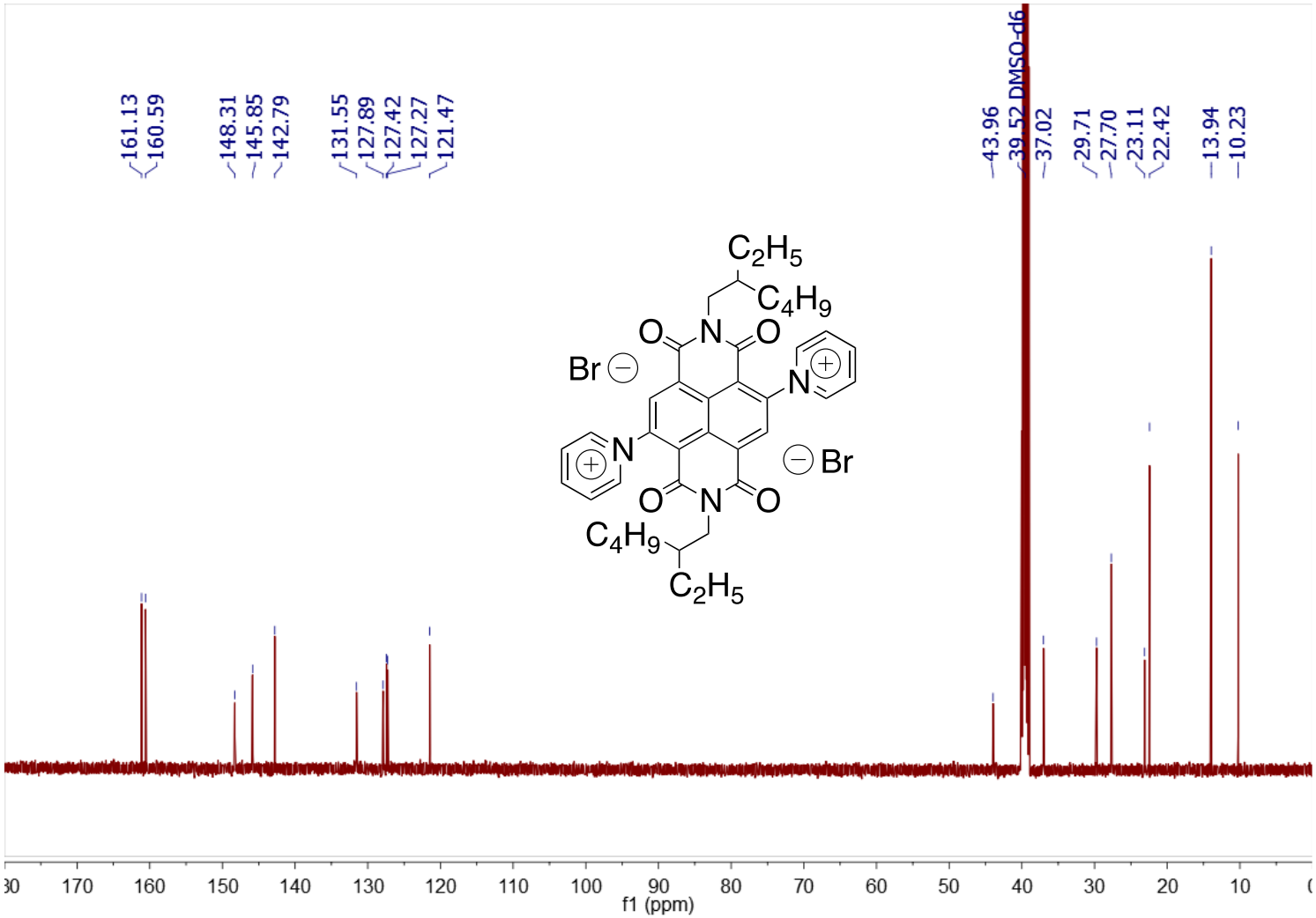

Figure S14. $^{13}C\{^{1}H\}$ NMR spectrum (500 MHz) of **Py$_2$-NDI•2Br** in DMSO-d_6.

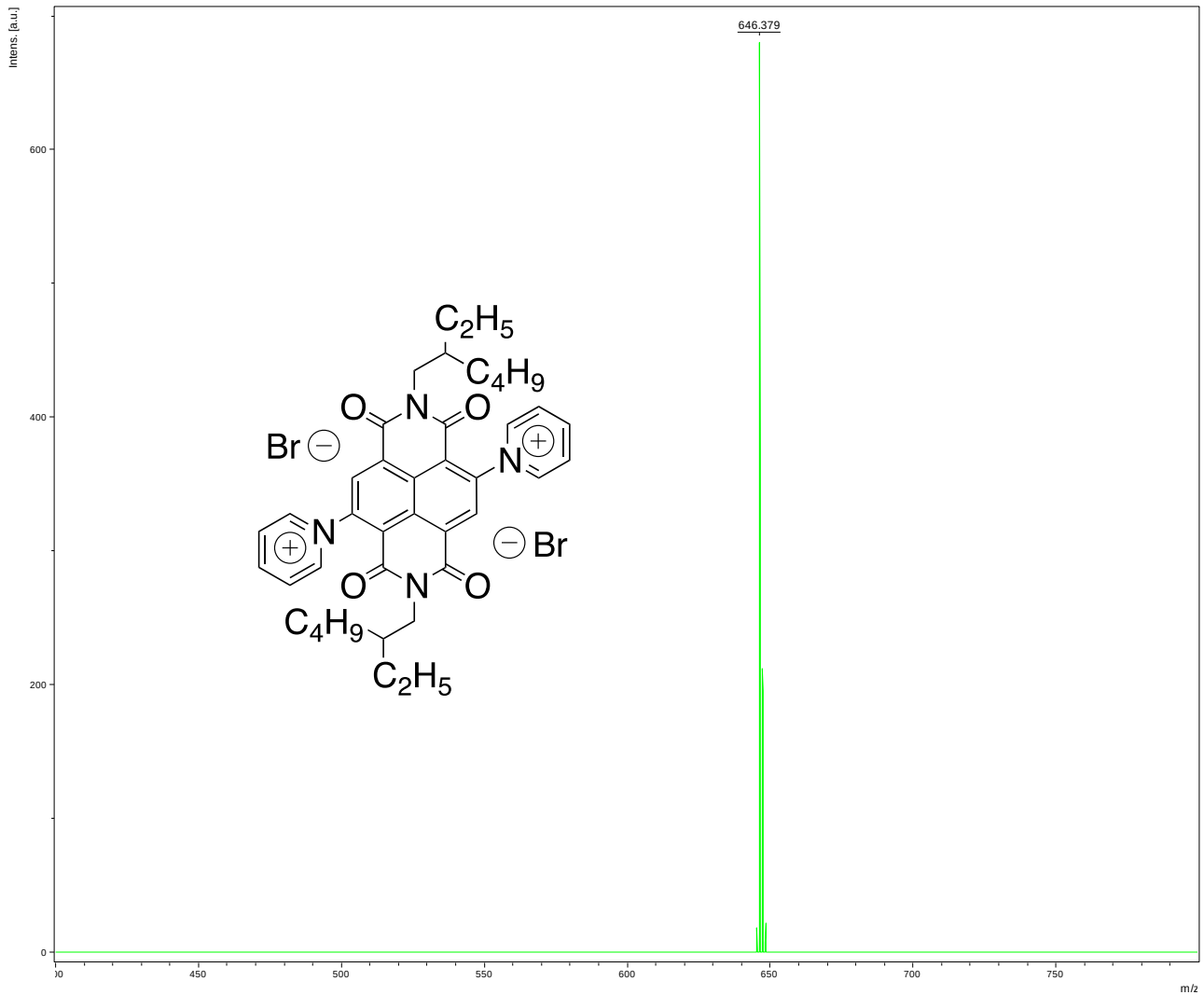

Figure S15. MALDI-TOF mass spectrum of **Py$_2$-NDI•2Br**. The M^+ corresponds to the Py$_2$-NDI^{2+}.

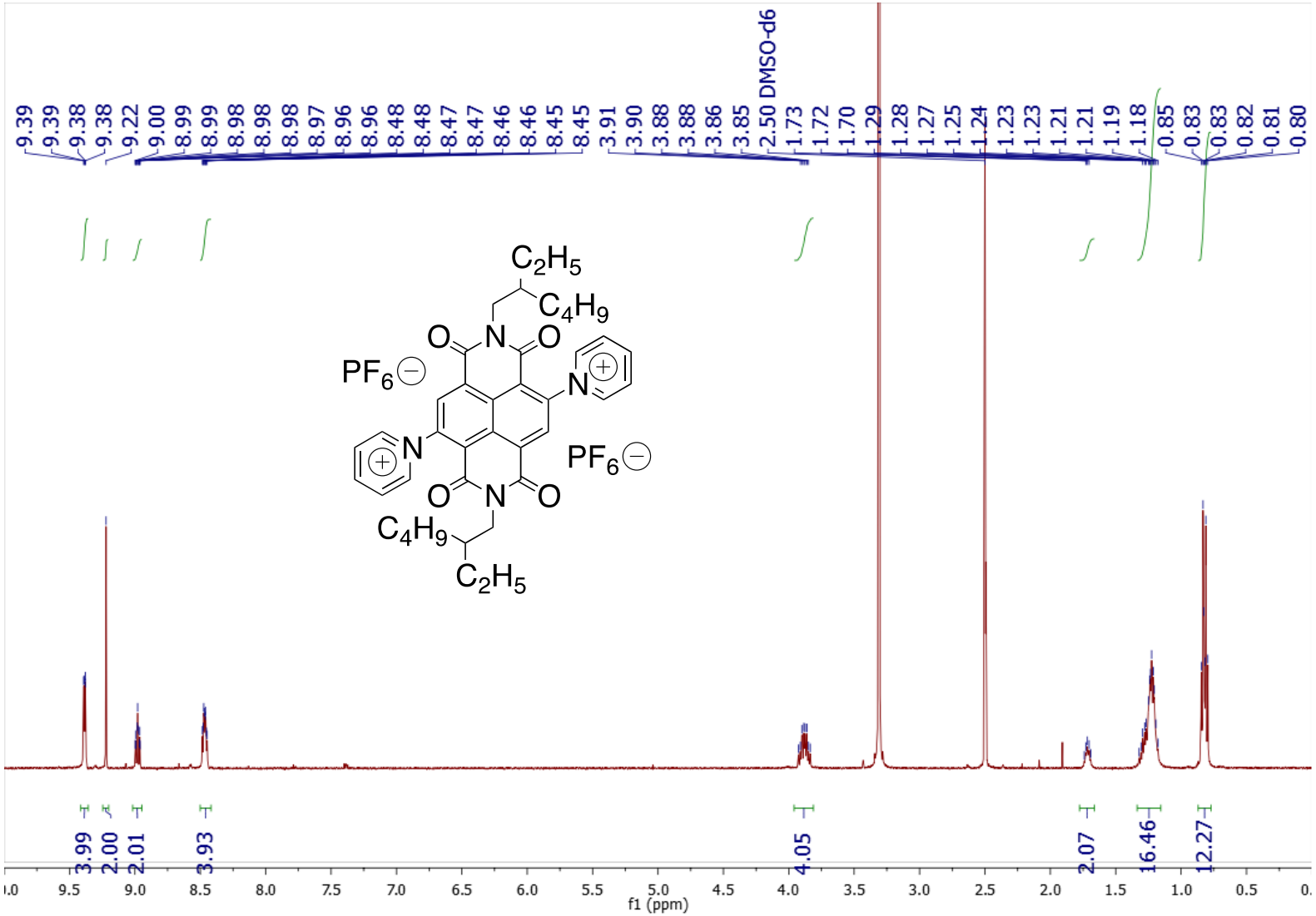

Figure S16. ^{1}H NMR spectrum (500 MHz) of **Py$_2$-NDI•2PF$_6$** in DMSO-*d*$_6$.

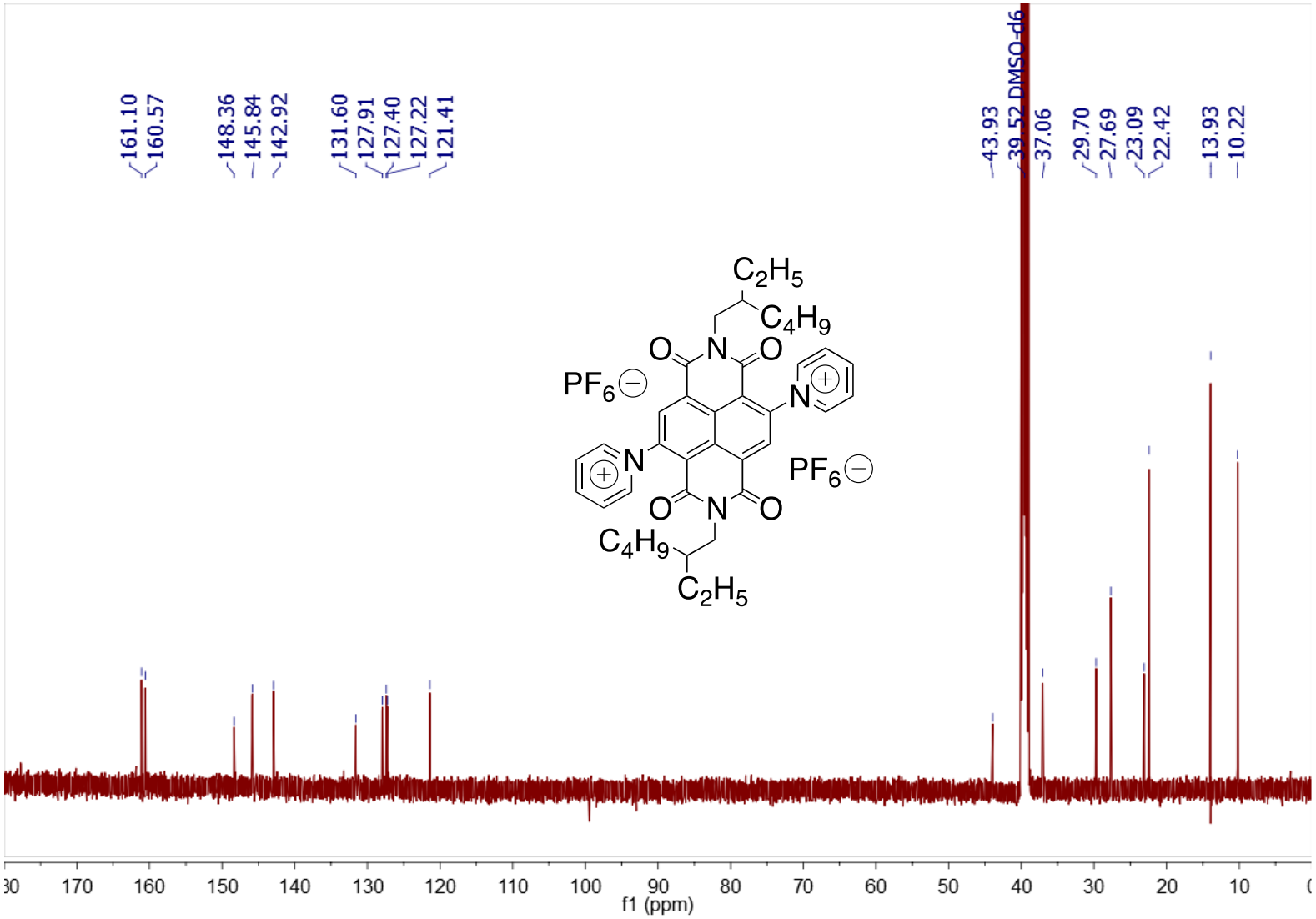

Figure S17. $^{13}C\{^{1}H\}$ NMR spectrum (500 MHz) of **Py$_2$-NDI•2PF$_6$** in DMSO-*d*$_6$.

Figure S18. MALDI-TOF mass spectrum of **Py_2-NDI•2PF_6**. The M^+ corresponds to the Py_2-NDI^{2+}.

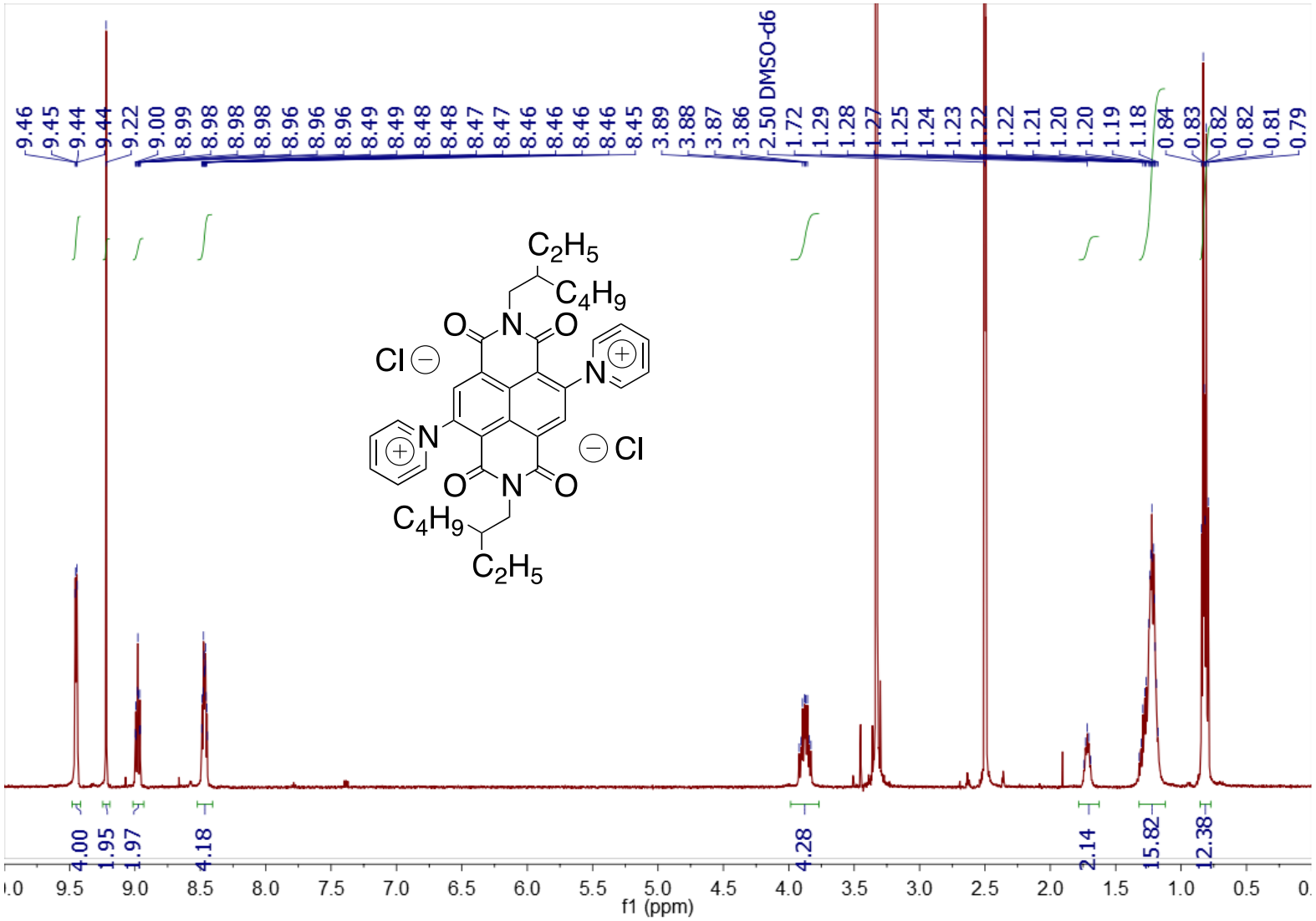

Figure S19. ^{1}H NMR spectrum (500 MHz) of **Py$_2$-NDI•2Cl** in DMSO-*d*$_6$.

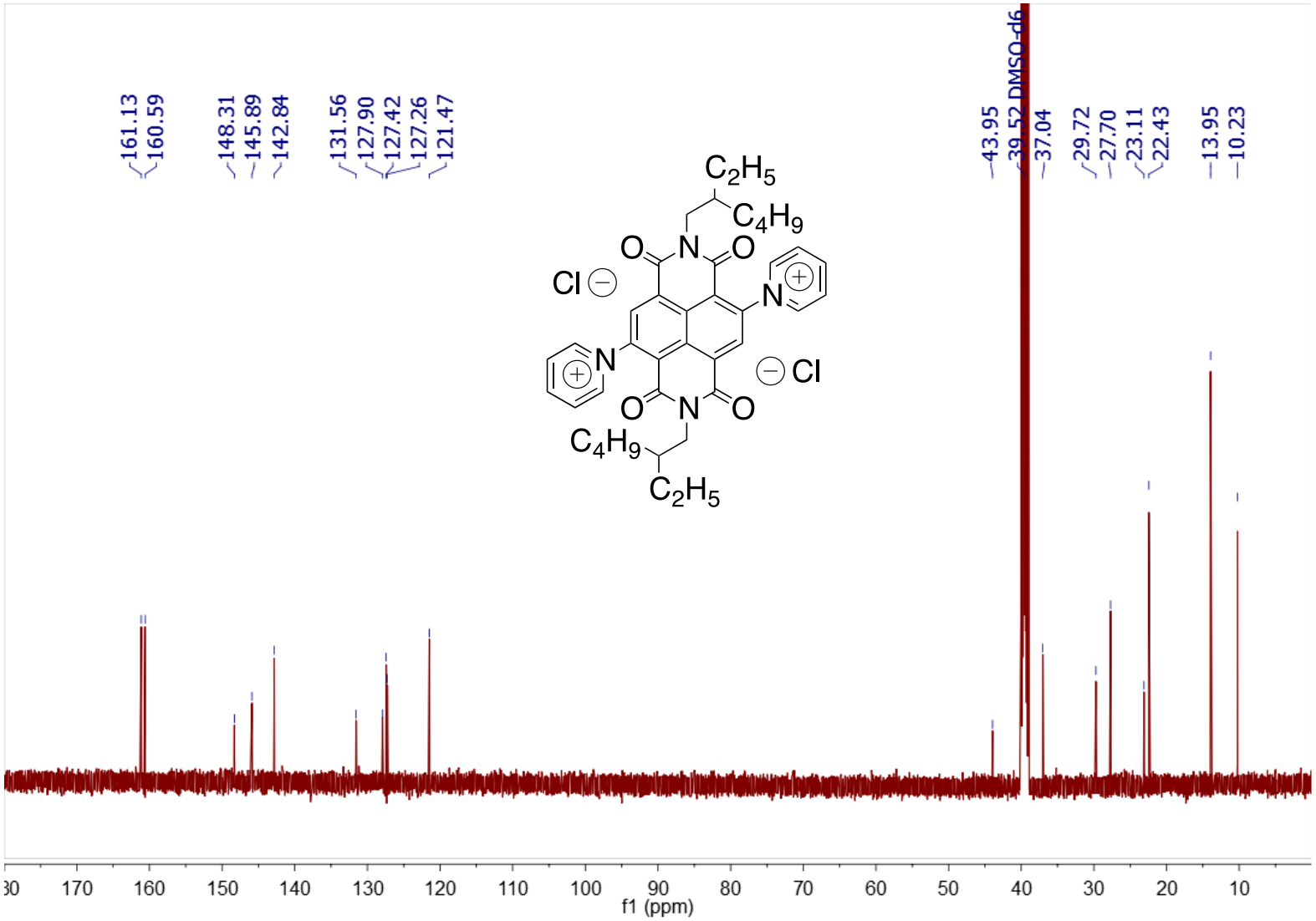

Figure S20. $^{13}C\{^{1}H\}$ NMR spectrum (500 MHz) of **Py$_2$-NDI•2Cl** in DMSO-d_6.

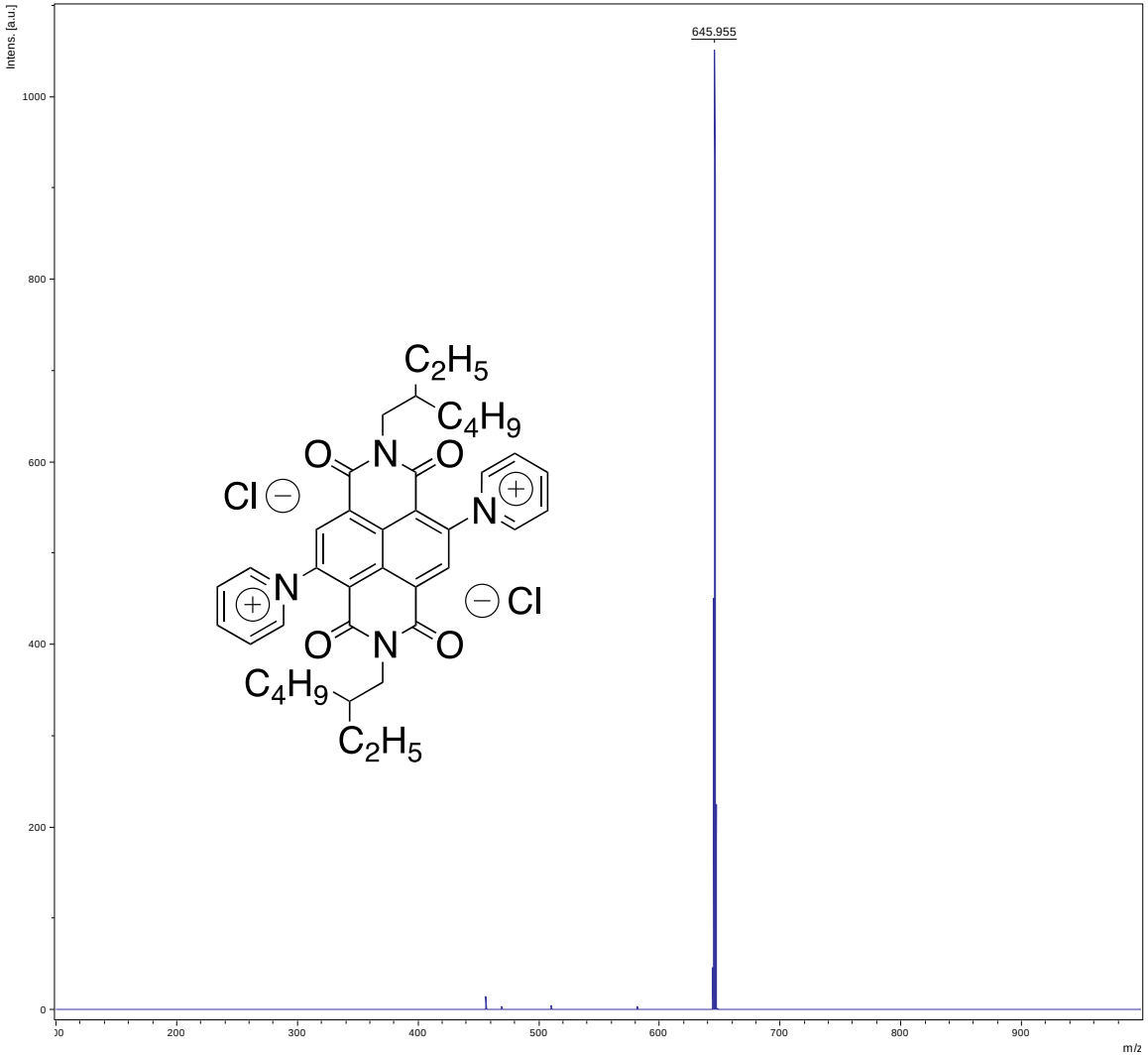

Figure S21. MALDI-TOF mass spectrum of **Py$_2$-NDI•2Cl**. The M^+ corresponds to the Py$_2$-NDI^{2+}.

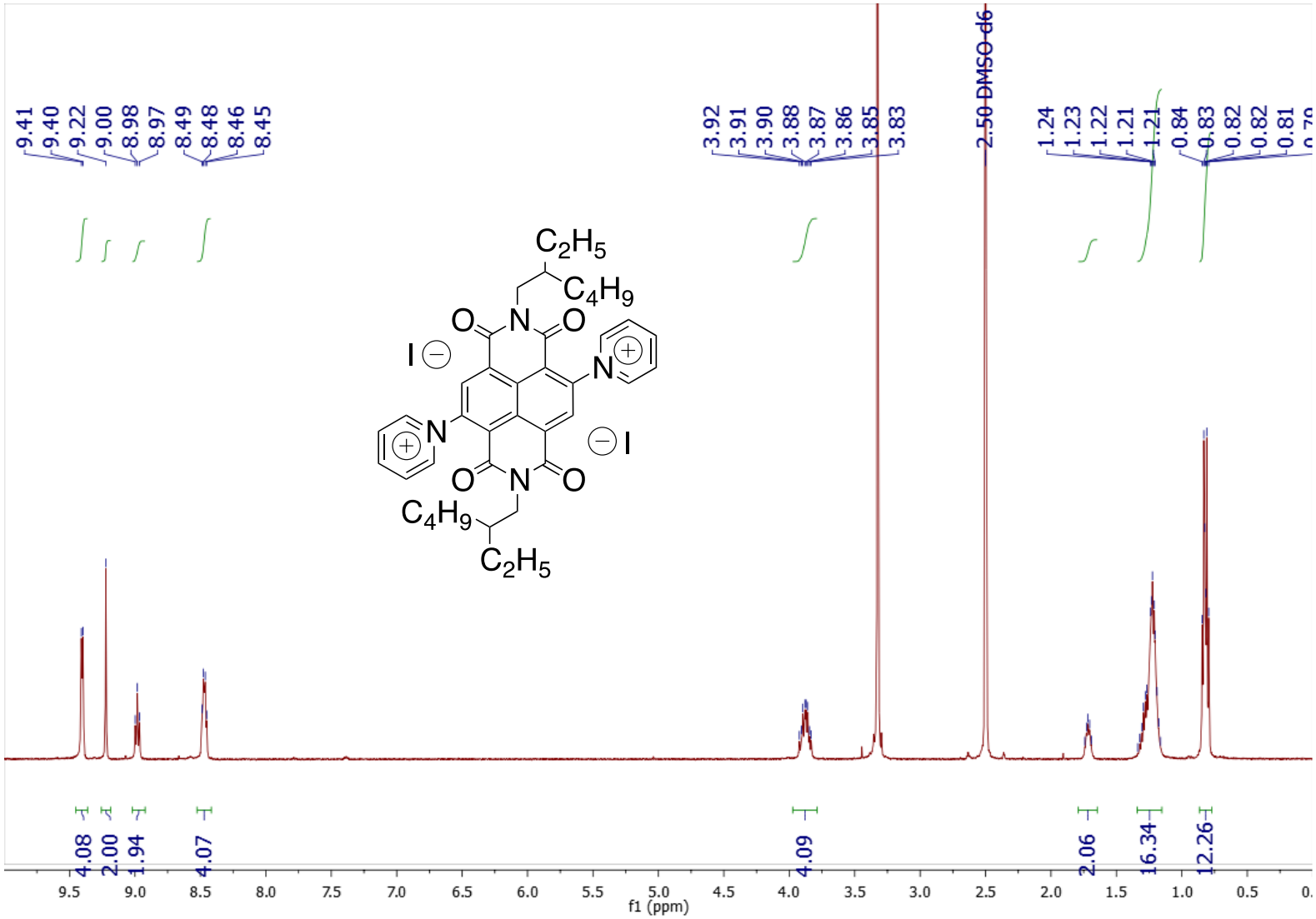

Figure S22. ^{1}H NMR spectrum (500 MHz) of **Py$_2$-NDI•2I** in DMSO-*d*$_6$.

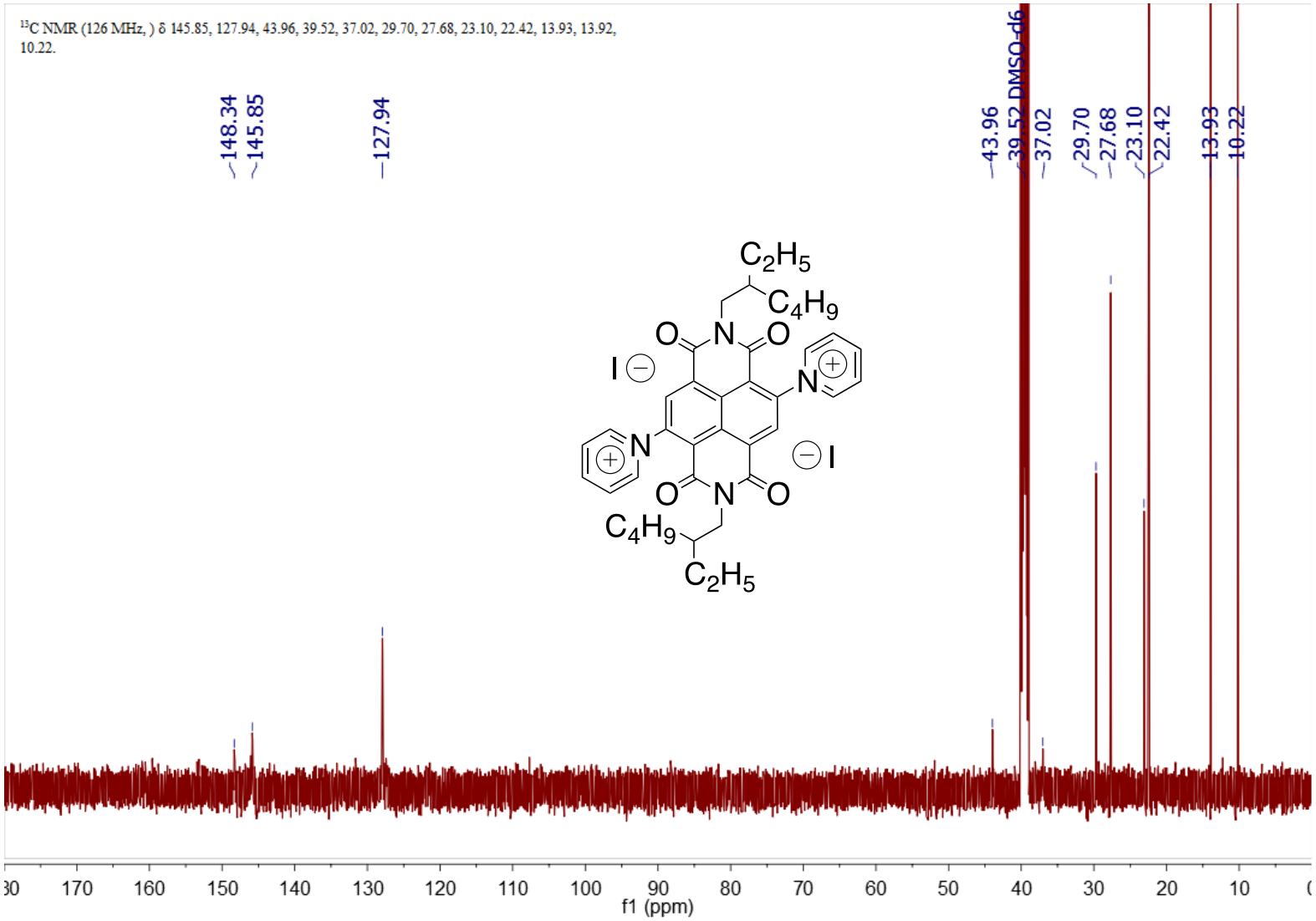

Figure S23. $^{13}C\{^{1}H\}$ NMR spectrum (500 MHz) of **Py2-NDI•2I** in DMSO-*d6*.

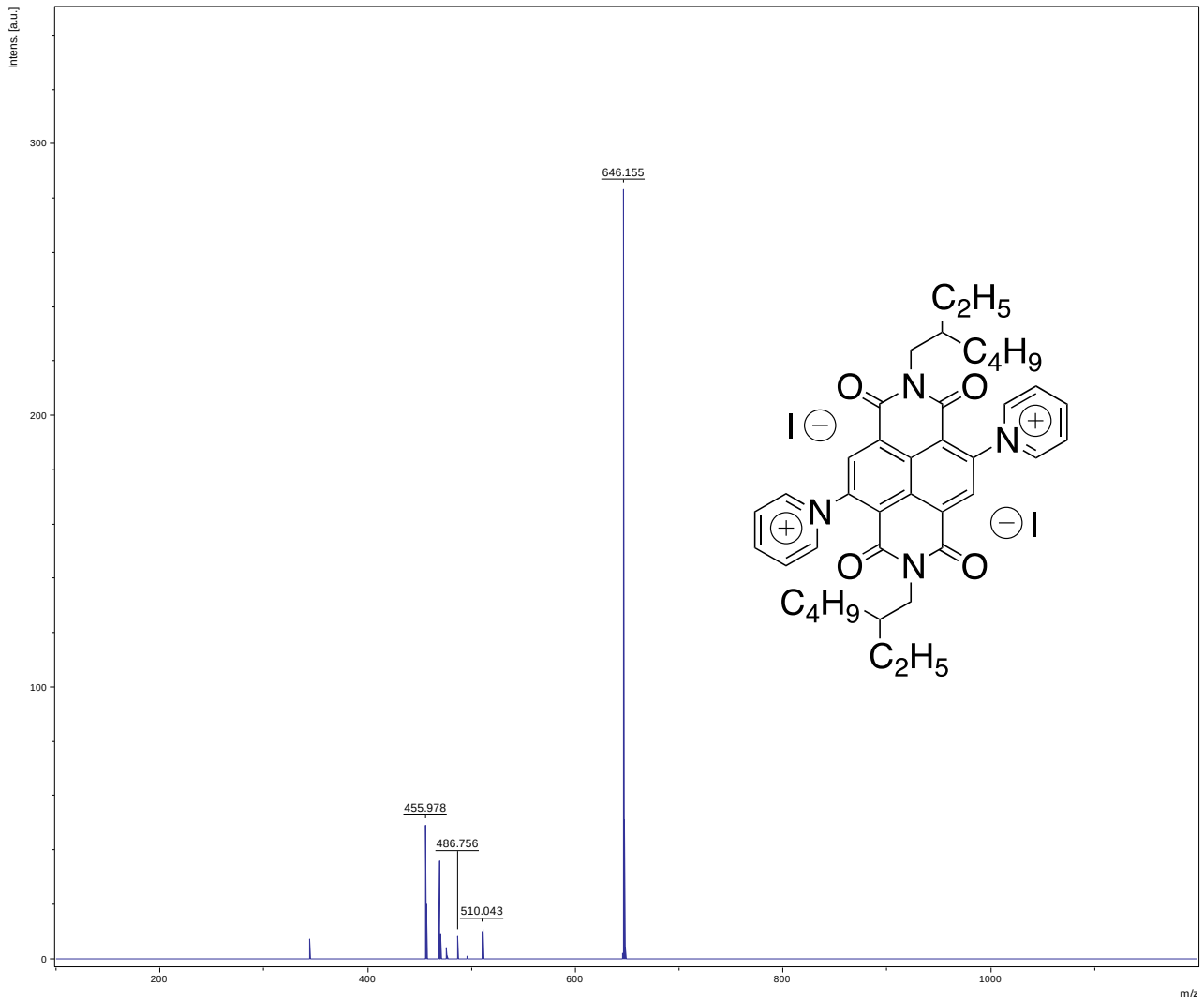

Figure S24. MALDI-TOF mass spectrum of **Py$_2$-NDI•2I**. The M^+ corresponds to the Py$_2$-NDI^{2+}.

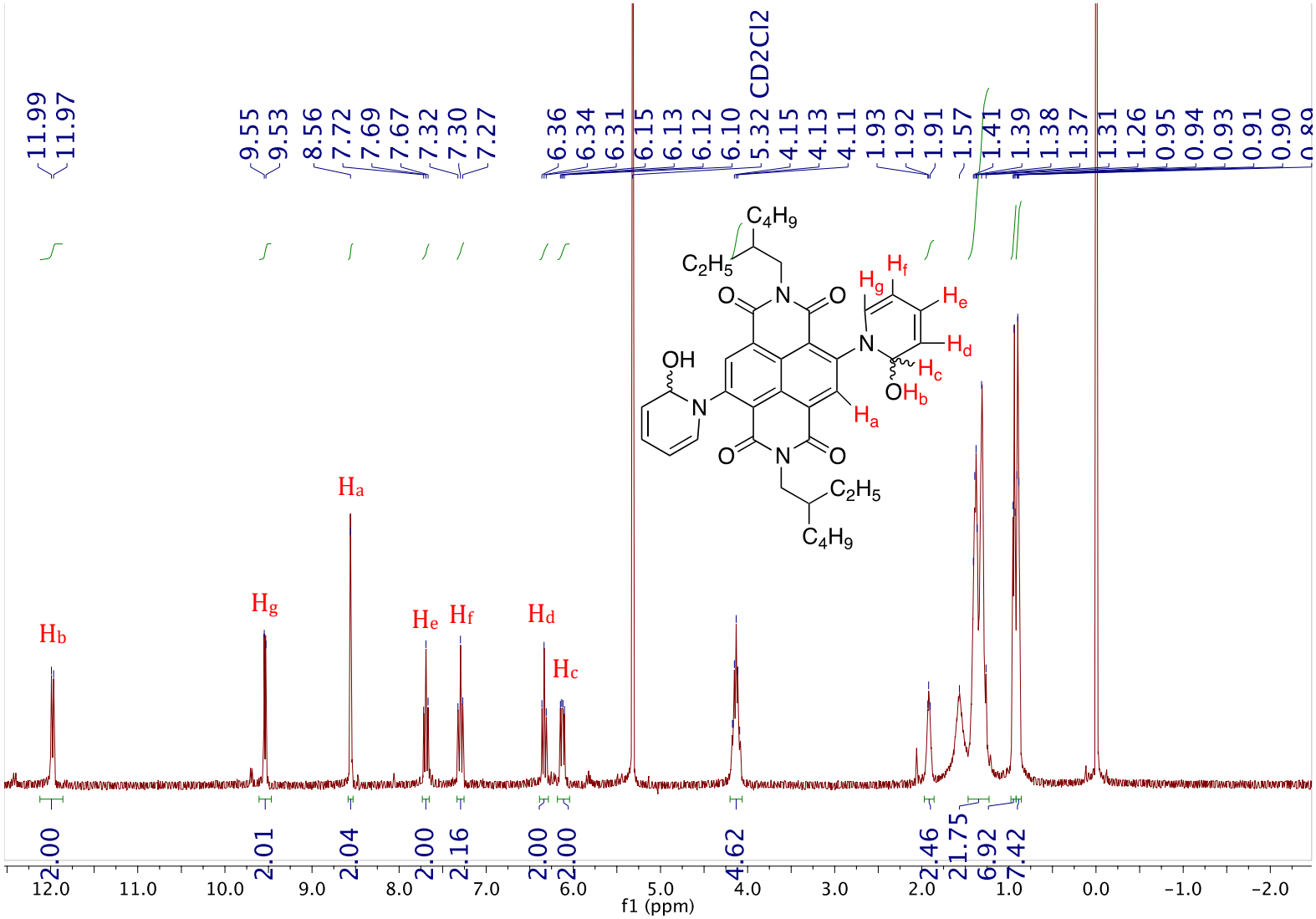

Figure S25. ^{1}H NMR spectrum (500 MHz) of **Py$_2$-NDI•2OH** in CD_2Cl_2.

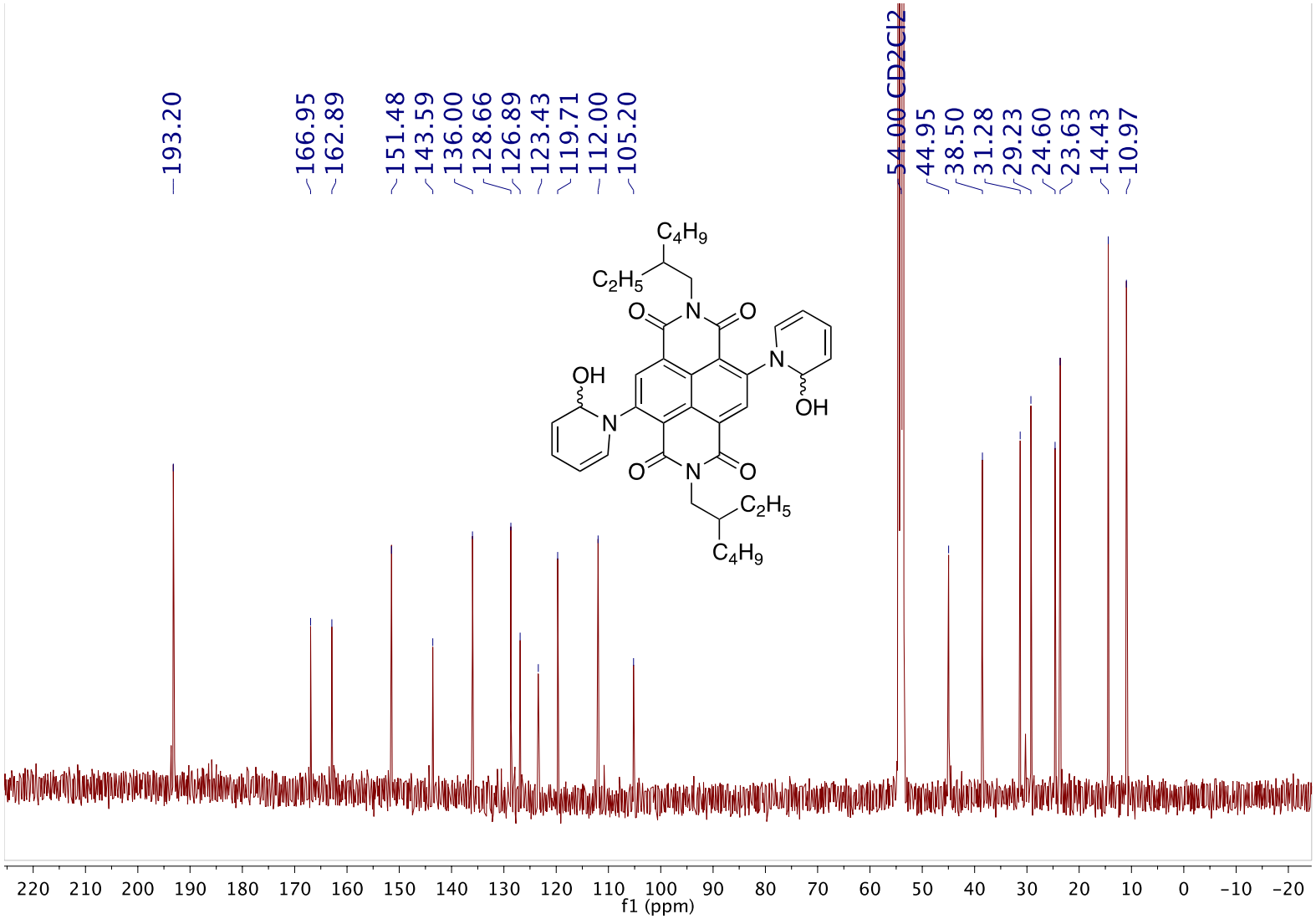

Figure S26. $^{13}C\{^{1}H\}$ NMR spectrum (500 MHz) of **Py$_2$-NDI•2OH** in CD_2Cl_2.

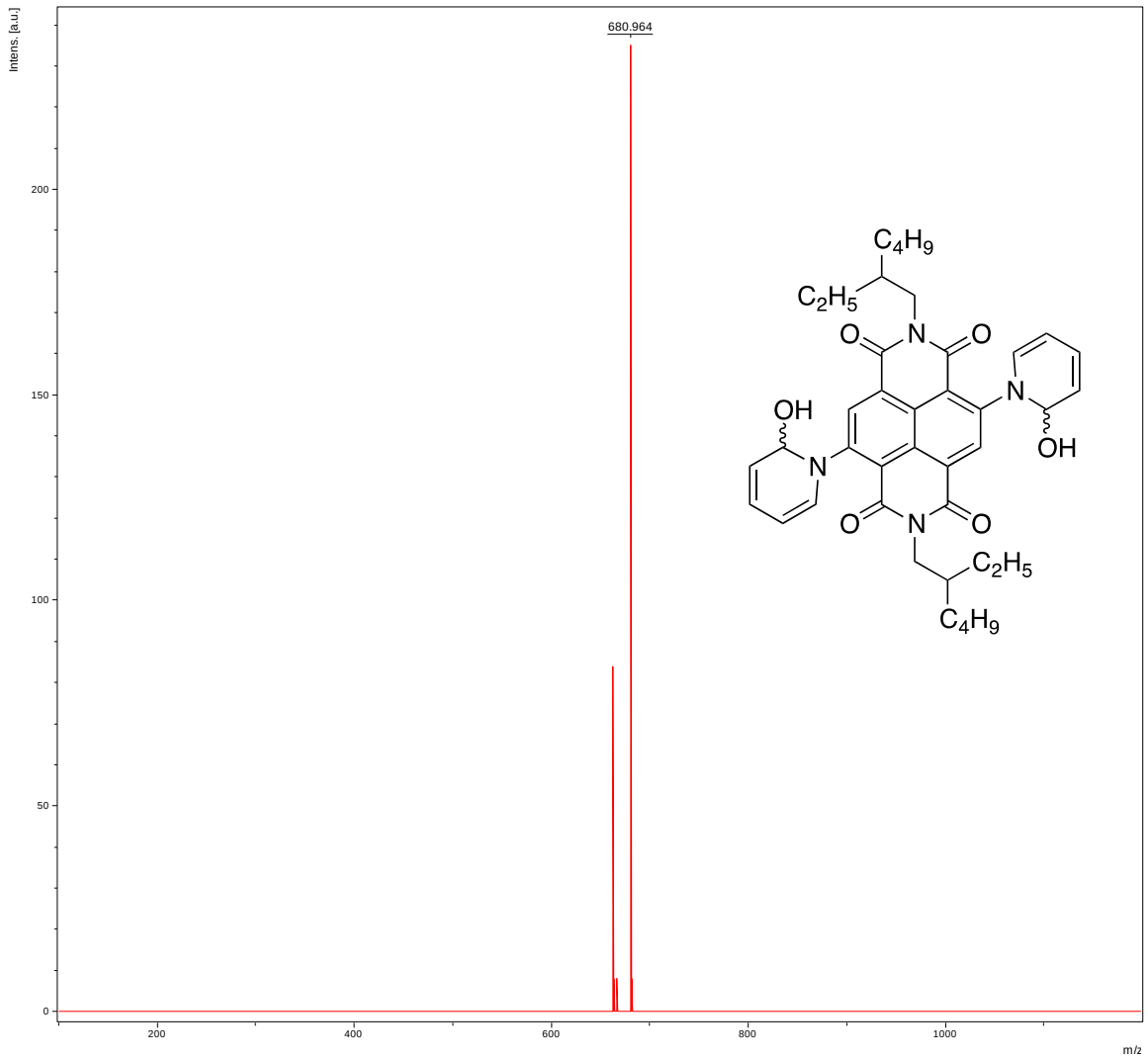

Figure S27. MALDI-TOF mass spectrum of **Py$_2$-NDI•2OH**.

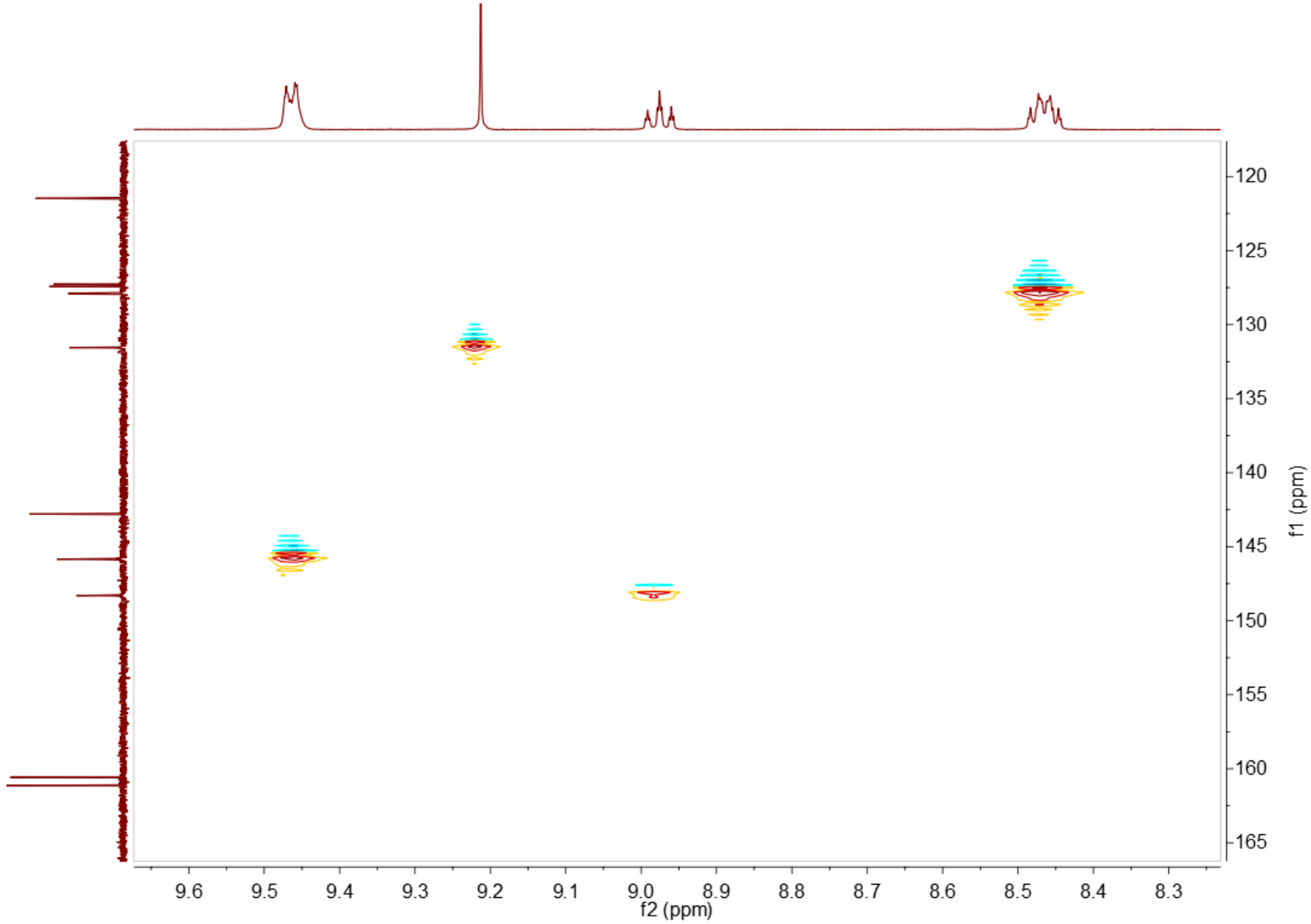

Figure S28. ^{1}H-^{13}C heteronuclear single quantum correlation (HSQC) of **Py$_2$-NDI•2Br** in DMSO-*d$_6$*

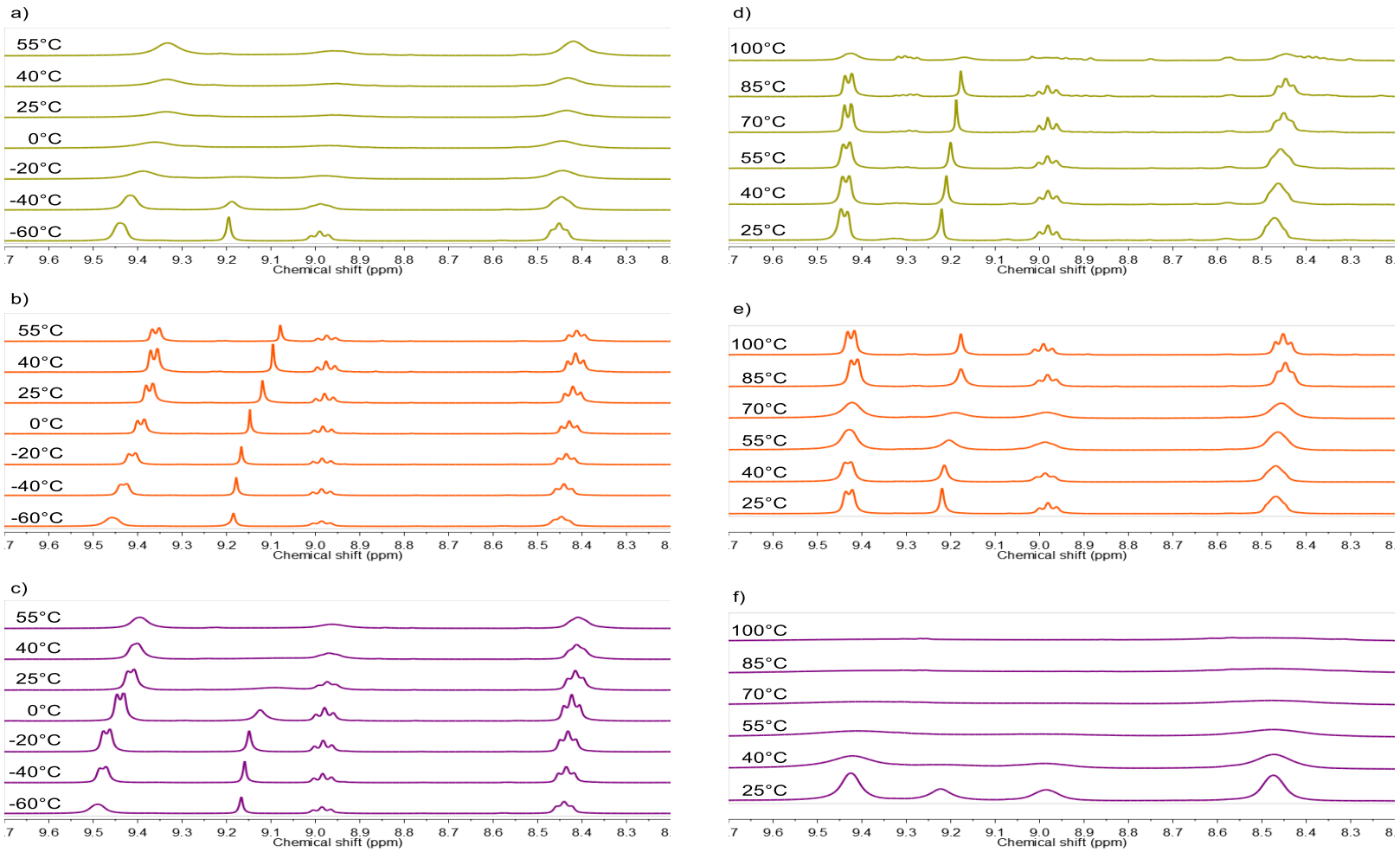

Figure S29. Variable-temperature ^{1}H NMR (400 MHz) spectra of a & d) Py_2-NDI•2Cl, b & e) Py_2-NDI•2Br and c & f) Py_2-NDI•2I. Left – in methanol-d4, –60 °C to 55 °C. Right – in DMSO-d6, 25 °C to 100 °C. Degradation was observed at 100 °C for Py_2-NDI•2Cl, and above 100 °C for Py_2-NDI•2PF_6, Py_2-NDI•2Br and Py_2-NDI•2I (see Figure S29 – S33).

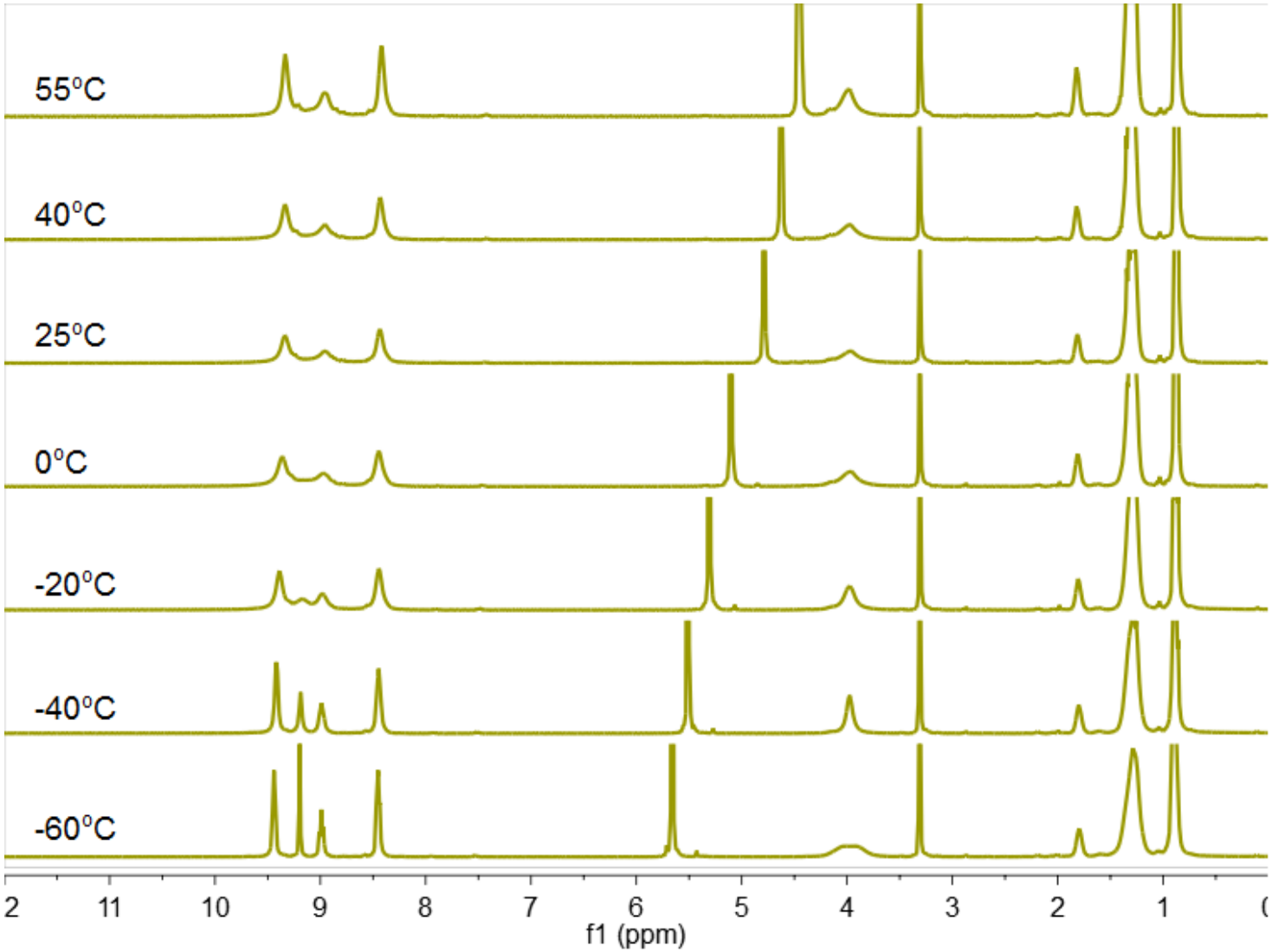

Figure S30. Variable temperature NMR (400 MHz) of **Py$_2$-NDI•2Cl** in methanol-d_4.

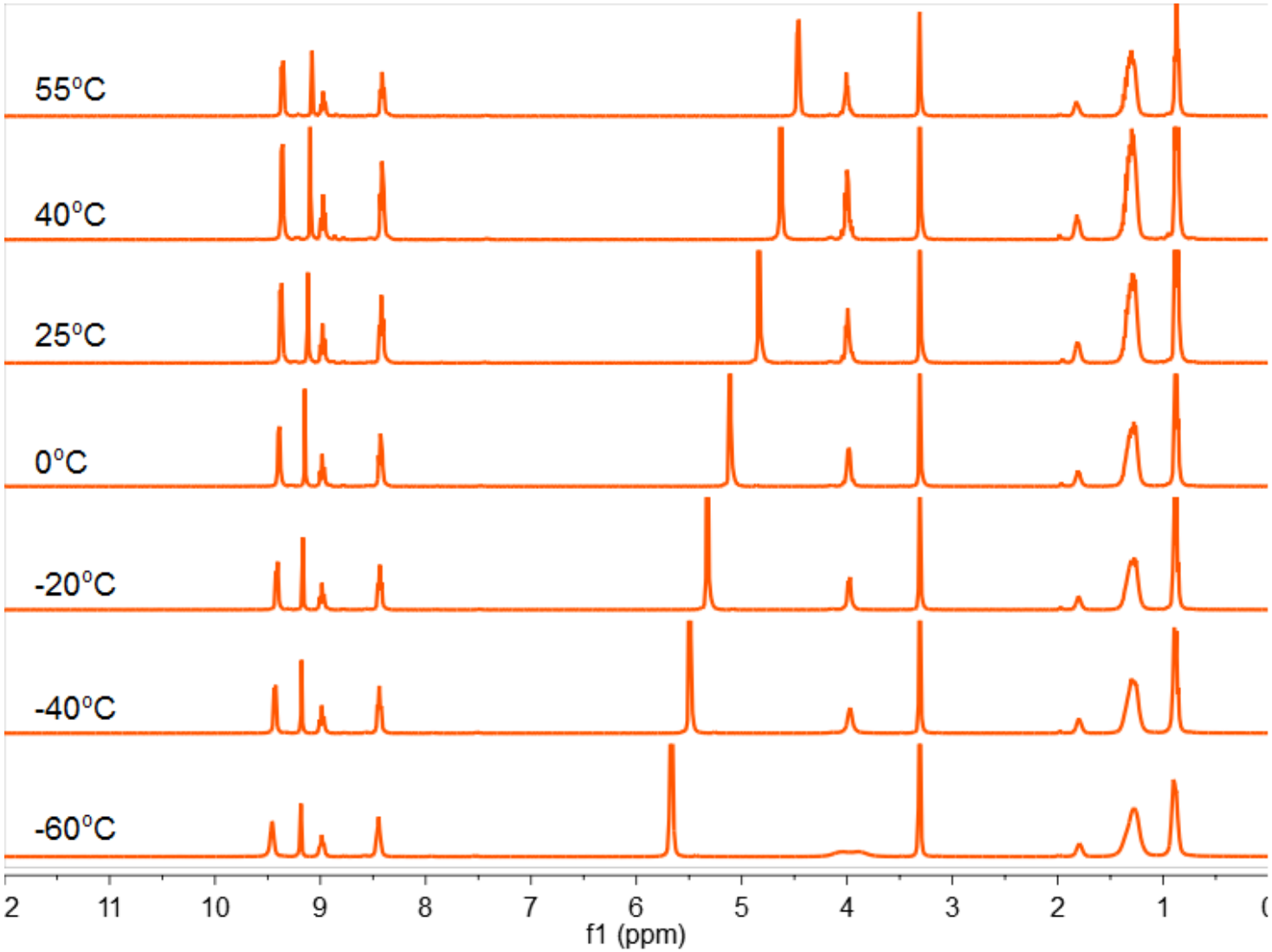

Figure S31. Variable temperature NMR (400 MHz) of **Py$_2$-NDI•2Br** in methanol-d_4.

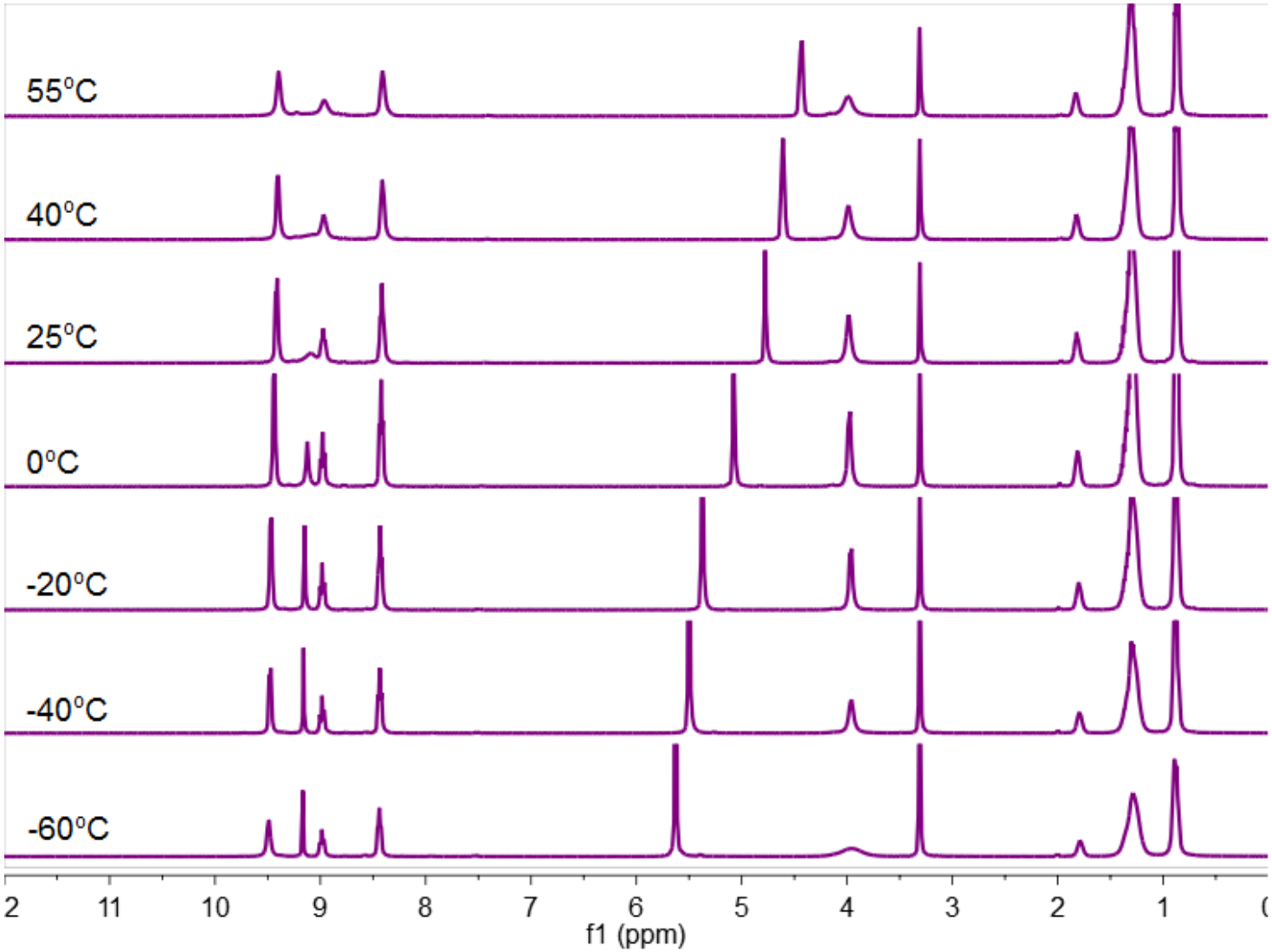

Figure S32. Variable temperature NMR (400 MHz) of **Py$_2$-NDI•2I** in methanol-d_4.

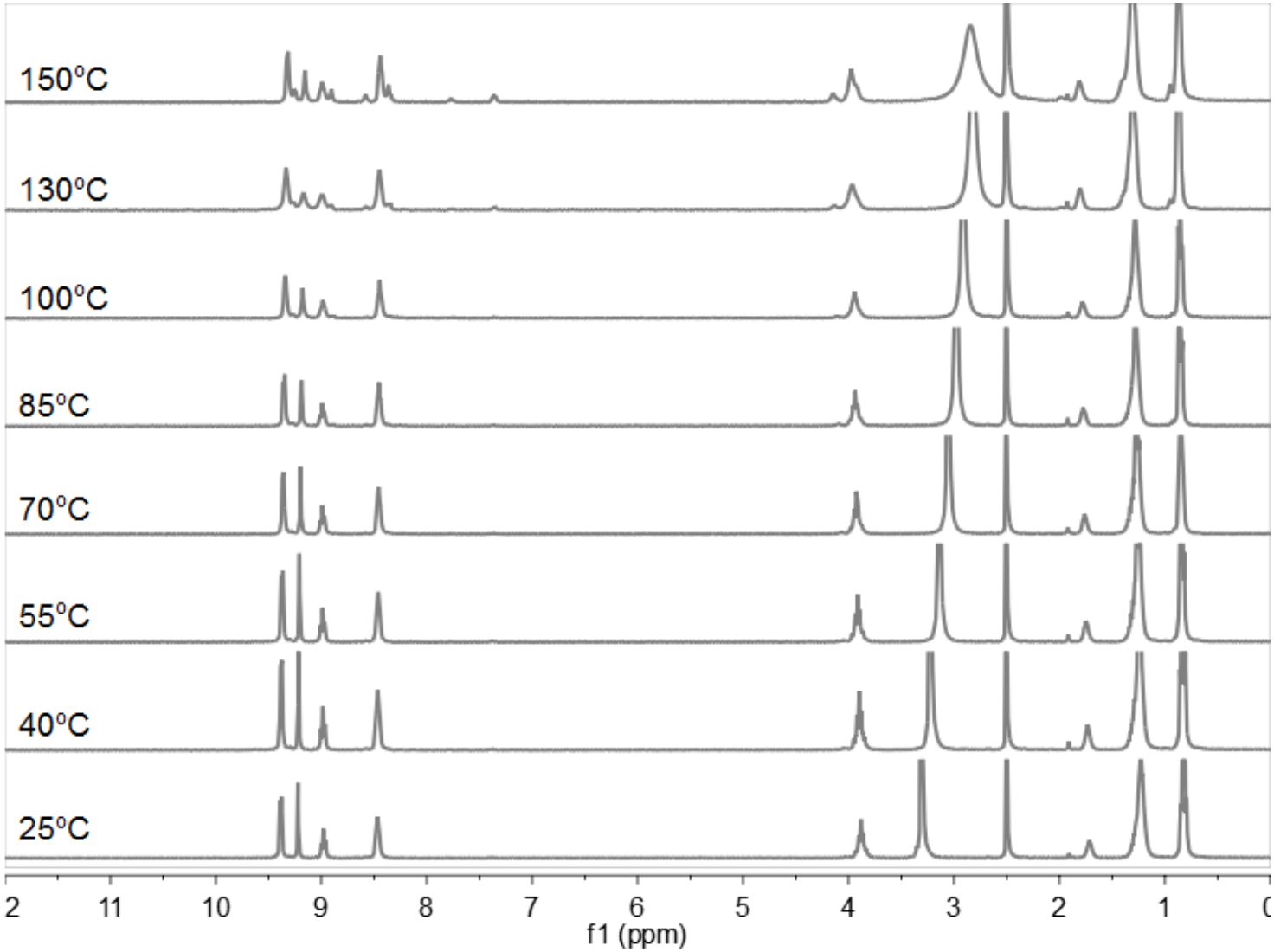

Figure S33. Variable temperature NMR (400 MHz) of **Py$_2$-NDI•2PF$_6$** in DMSO-d_6.

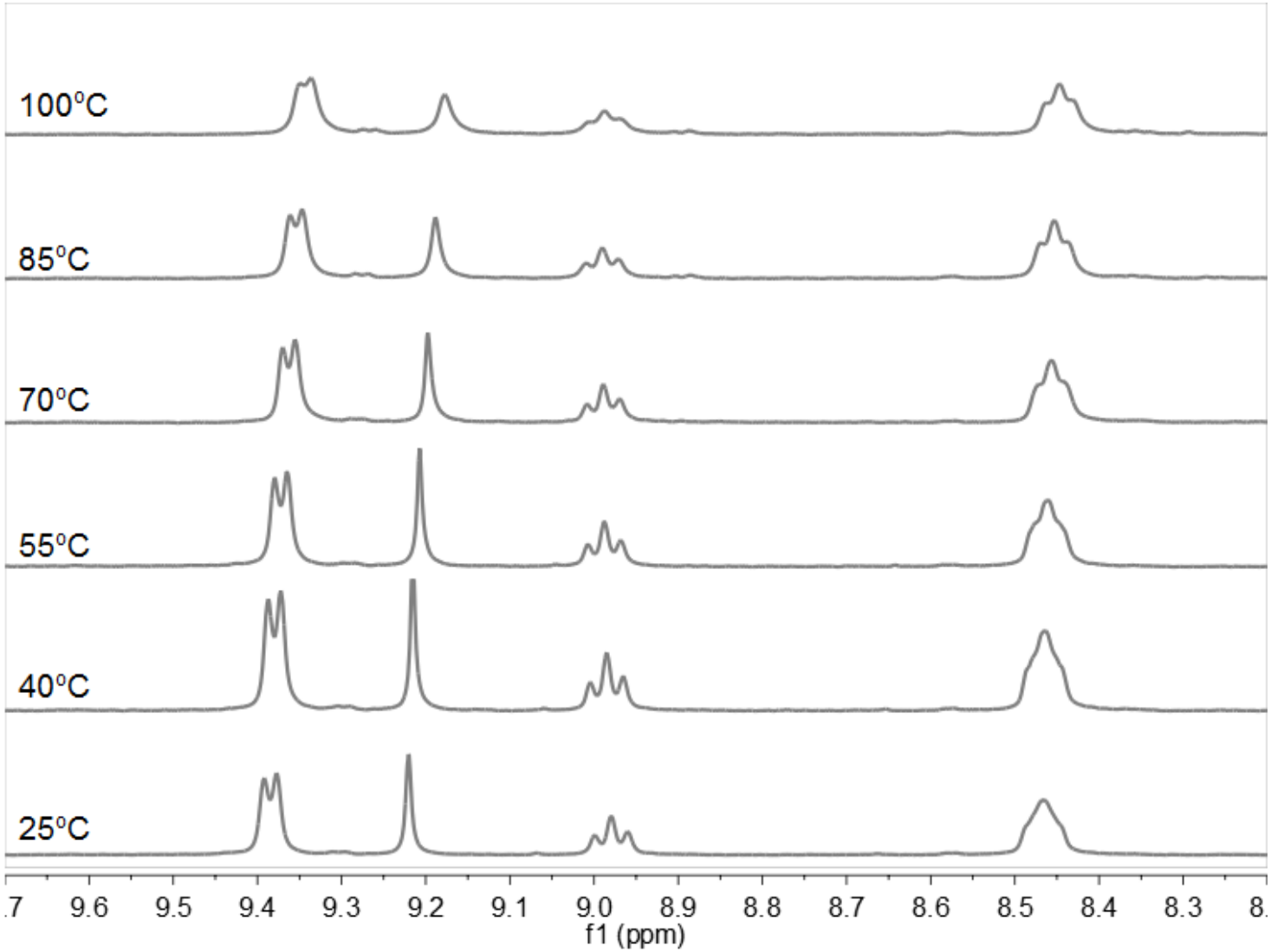

Figure S34. Aromatic proton region of the variable temperature NMR (400 MHz) of **Py$_2$-NDI•2PF$_6$** in DMSO-d_6.

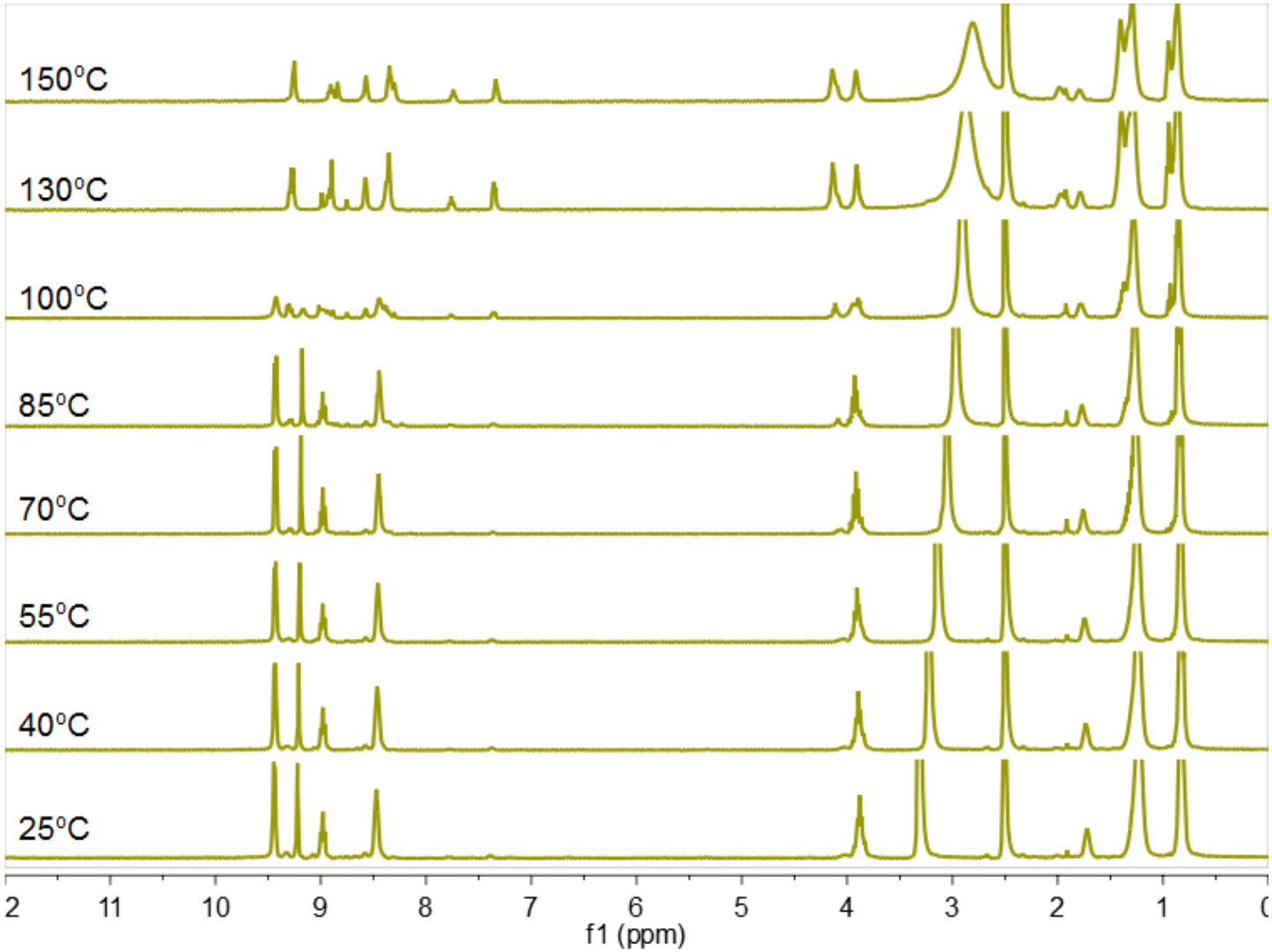

Figure S35. Variable temperature NMR (400 MHz) of **Py$_2$-NDI•2Cl** in DMSO-d_6.

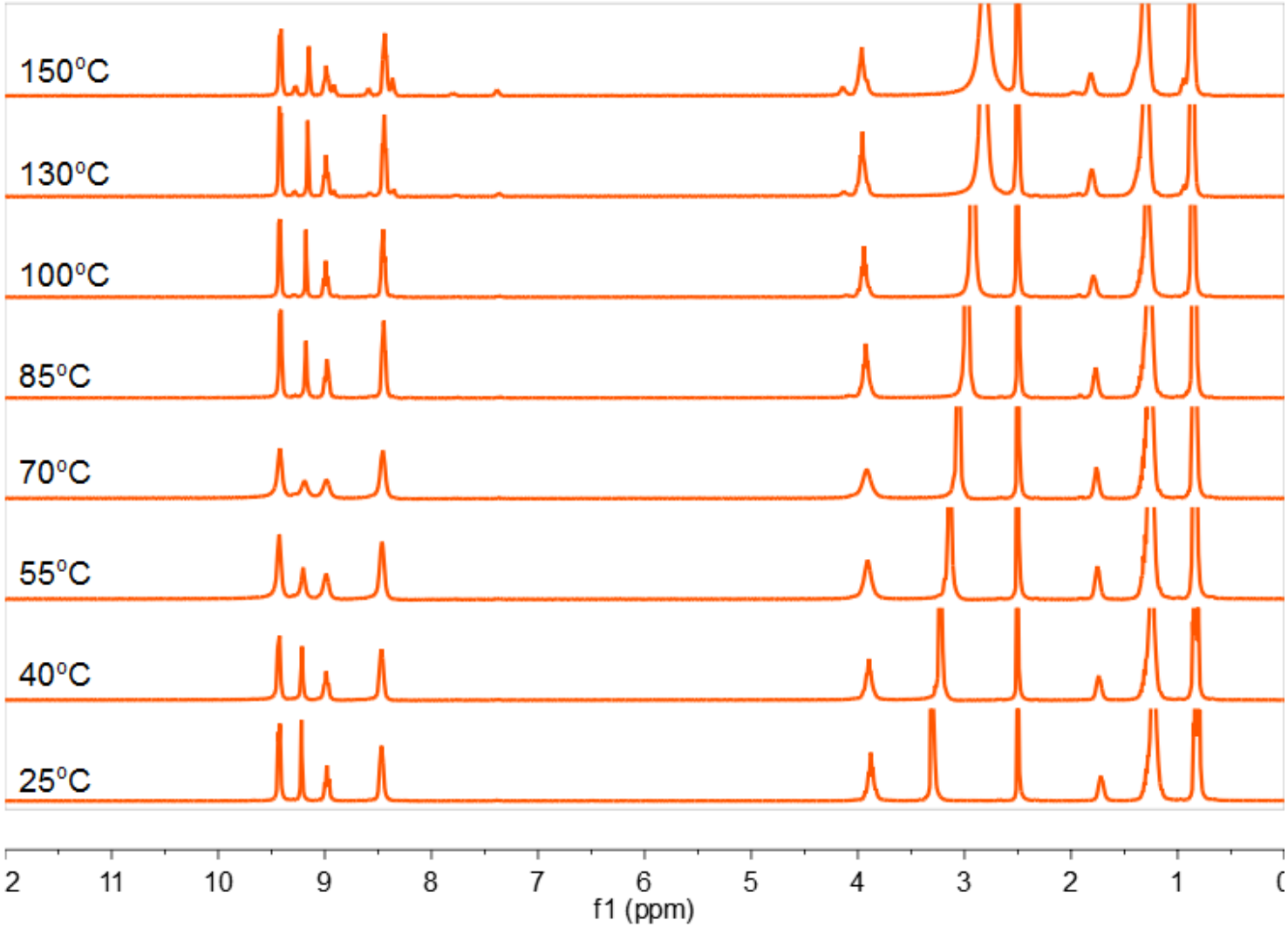

Figure S36. Variable temperature NMR (400 MHz) of **Py$_2$-NDI•2Br** in DMSO-d_6.

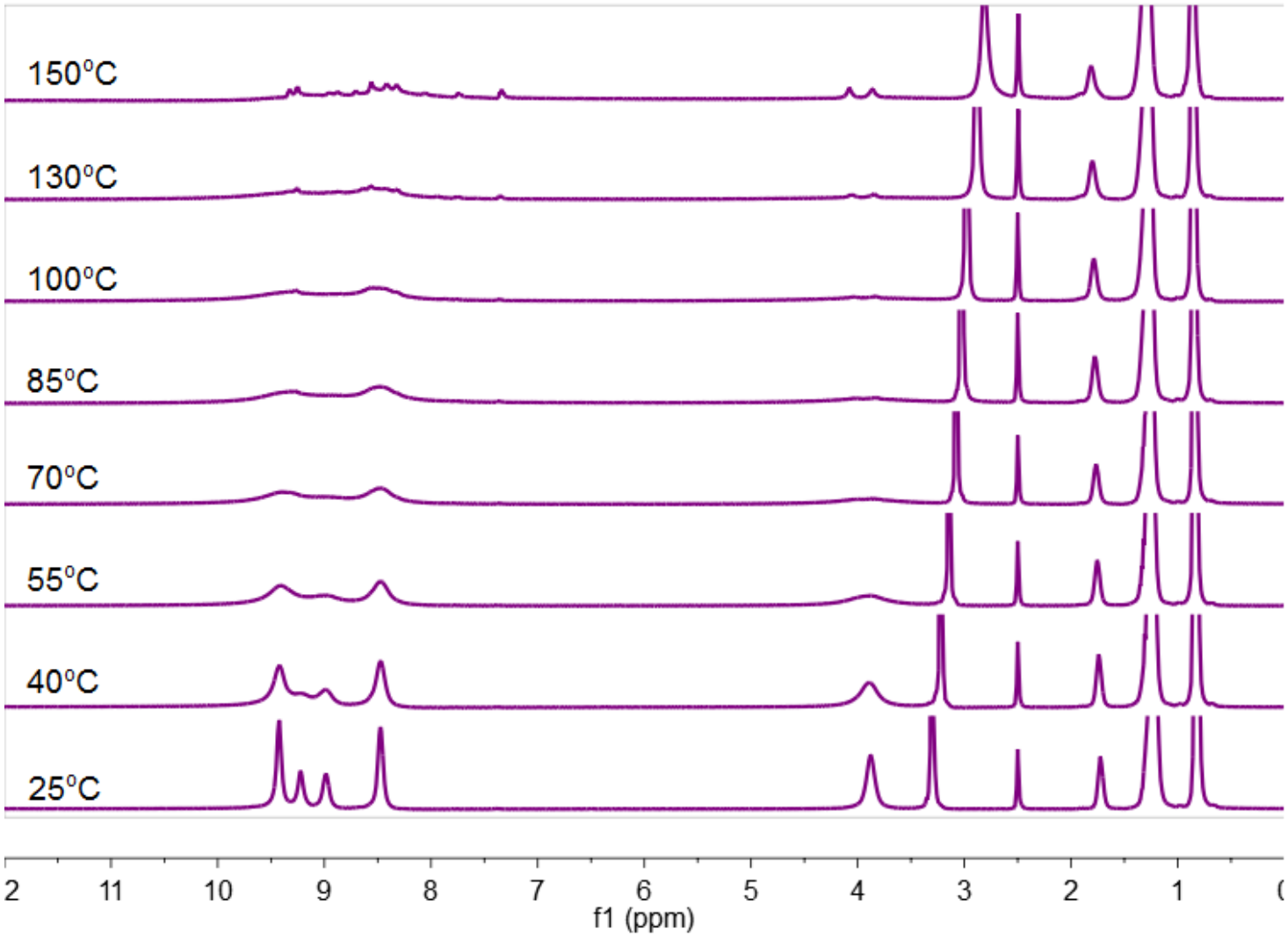

Figure S37. Variable temperature NMR (400 MHz) of **Py$_2$-NDI•2I** in DMSO-d_6.

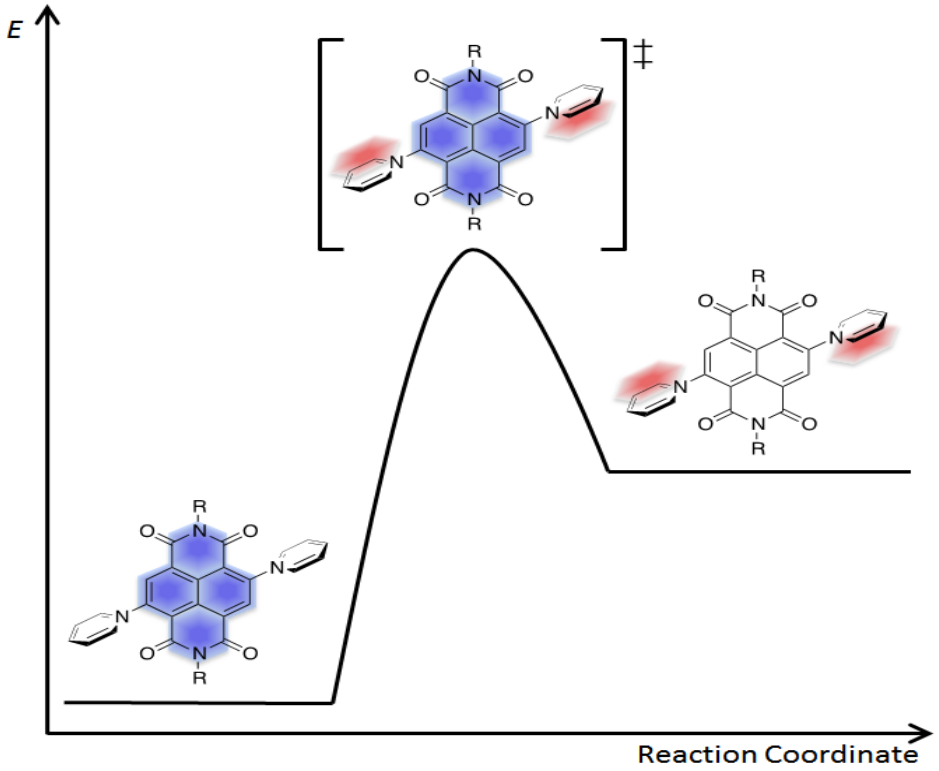

Figure S38. Proposed energy diagram of anion shuttling for the Py_2-NDI^{2+} salts. The blue and red regions indicate the region where the anions are likely to be found.

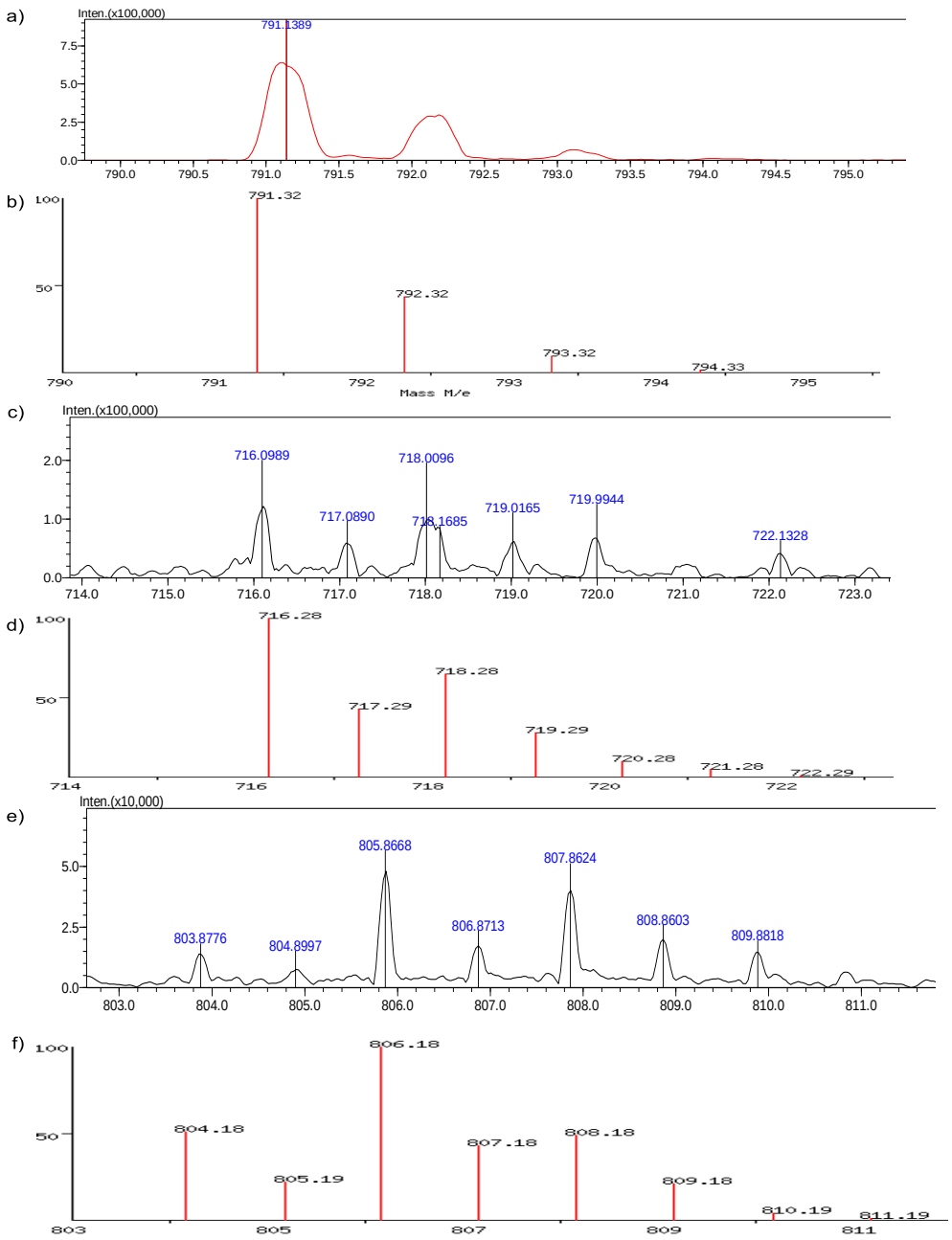

Figure S39. (a) ESI-MS (positive mode) of experimental isotopic distribution pattern of $[Py_2\text{-NDI}\bullet PF_6]^+$. (b) Predicted isotopic distribution for $[Py_2\text{-NDI}\bullet PF_6]^+$. (c) ESI-MS (negative mode) of experimental isotopic distribution pattern of $[Py_2\text{-NDI}\bullet 2Cl]^-$. (d) Predicted isotopic distribution for $[Py_2\text{-NDI}\bullet 2Cl]^-$. (e) ESI-MS (negative mode) of experimental isotopic distribution pattern of $[Py_2\text{-NDI}\bullet 2Br]^-$. (f) Predicted isotopic distribution for $[Py_2\text{-NDI}\bullet 2Br]^-$.

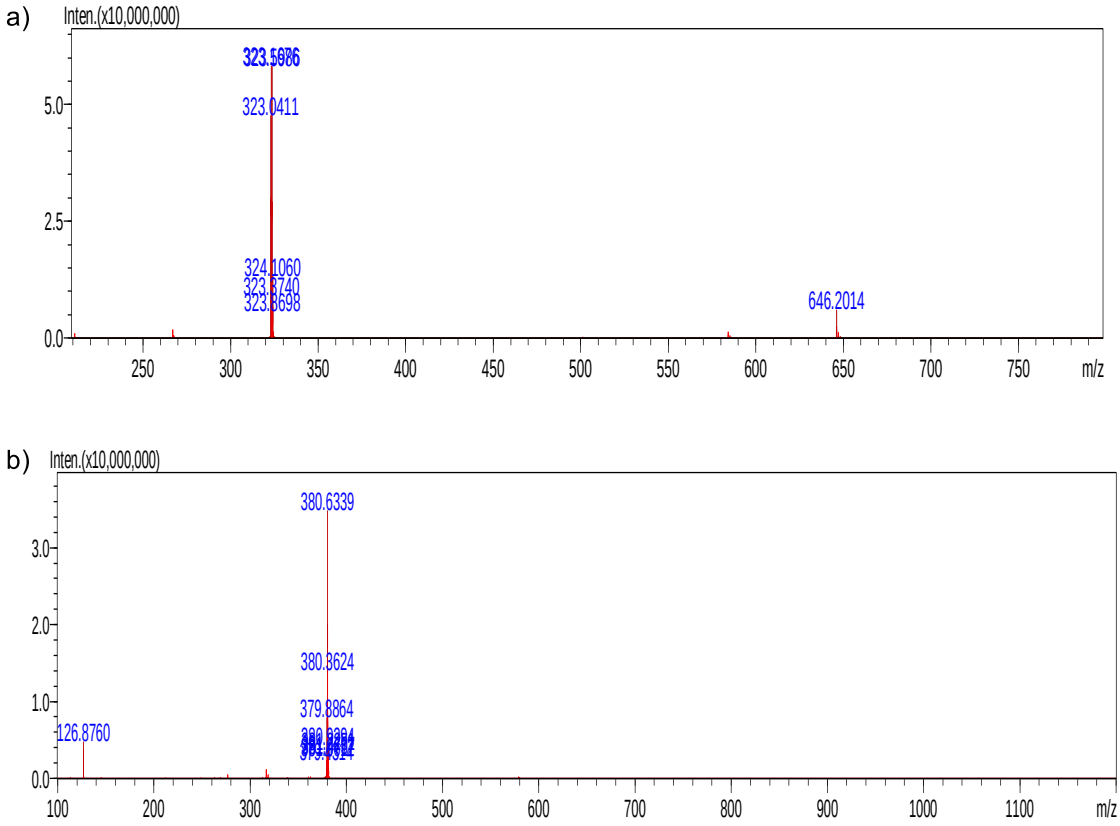

Figure S40. (a) ESI-MS (positive mode) of experimental isotopic distribution pattern of Py_2-NDI•2I which shows $[Py_2\text{-NDI}]^{2+}$ at 323.50 and $[Py_2\text{-NDI}]^{+}$ at 646.20. (b) ESI-MS (negative) of experimental isotopic distribution pattern of **Py_2-NDI•2I** which shows mostly I_3^- at 380.63 with a small amount of I^- at 126.88.

AC & DC Resistance Measurements

The Py_2-NDI^{2+} salts were pressed into pellets (diameter 6mm) with aluminium foil as the electrodes. AC resistance measurements were carried out using Autolab potentiostat (model PGSTAT30) by Echochimie at a 50 mV RMS. DC resistance measurements were carried out using Fluke 289 True RMS Multimeter.

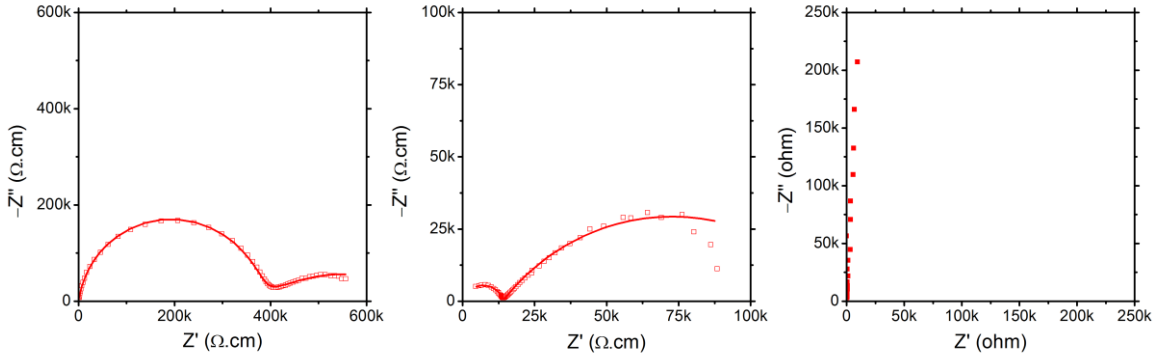

Figure S41. AC impedance measurement of Py_2-NDI.2Cl (left), Py_2-NDI.2Br (middle) and Py_2-NDI.2PF_6 (right).

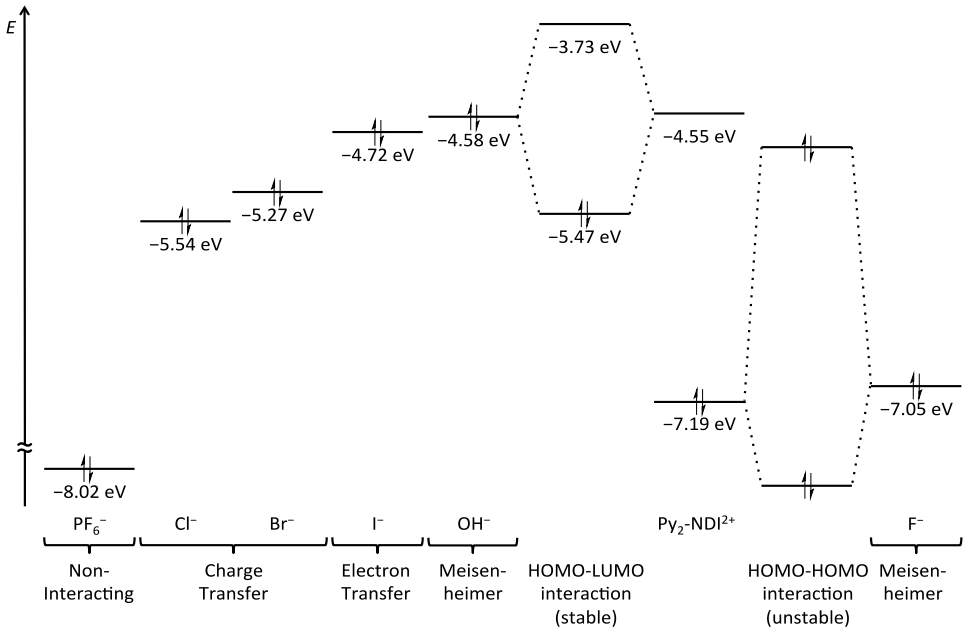

Figure S42. A summary of the nature of anion-π interactions of the Py_2-NDI^{2+} salts in terms of the HOMO value of the anion. HOMO value of Py_2-NDI^{2+} estimated from LUMO value and optical bandgap of Py_2-NDI•2PF_6. Upon exposure to water,

which is a source of OH^- ions, (HOMO = -4.58 eV), n-type organic semiconductors with low LUMO energy levels, e.g. PCBM (-4.2 eV) and C_{60} (-4.5 eV), will likely degrade via HOMO-LUMO interactions to form hydroxyl-containing Meisenheimer complexes.

6. References:

1. Frisch, M. J.; Trucks, G. W.; Schlegel, H. B.; Scuseria, G. E.; Robb, M. A.; Cheeseman, J. R.; Scalmani, G.; Barone, V.; Mennucci, B.; Petersson, G. A.; Nakatsuji, H.; Caricato, M.; Li, X.; Hratchian, H. P.; Izmaylov, A. F.; Bloino, J.; Zheng, G.; Sonnenberg, J. L.; Hada, M.; Ehara, M.; Toyota, K.; Fukuda, R.; Hasegawa, J.; Ishida, M.; Nakajima, T.; Honda, Y.; Kitao, O.; Nakai, H.; Vreven, T.; Montgomery, J. A., Jr.; Peralta, J. E.; Ogliaro, F.; Bearpark, M.; Heyd, J. J.; Brothers, E.; Kudin, K. N.; Staroverov, V. N.; Kobayashi, R.; Normand, J.; Raghavachari, K.; Rendell, A.; Burant, J. C.; Iyengar, S. S.; Tomasi, J.; Cossi, M.; Rega, N.; Millam, M. J.; Klene, M.; Knox, J. E.; Cross, J. B.; Bakken, V.; Adamo, C.; Jaramillo, J.; Gomperts, R.; Stratmann, R. E.; Yazyev, O.; Austin, A. J.; Cammi, R.; Pomelli, C.; Ochterski, J. W.; Martin, R. L.; Morokuma, K.; Zakrzewski, V. G.; Voth, G. A.; Salvador, P.; Dannenberg, J. J.; Dapprich, S.; Daniels, A. D.; Farkas, Ö.; Foresman, J. B.; Ortiz, J. V.; Cioslowski, J.; Fox, D. J. Gaussian 09, Revision A.02, Gaussian, Inc.: Wallingford CT, 2009.